Catena 236 (2024) 107705

Contents lists available at ScienceDirect

Catena

journal homepage: www.elsevier.com/locate/catena

Spatial distribution patterns of dated landslide events in the Northern Apennines in response to Holocene regional climatic changes

Giovanni Leonelli *, Alessandro Chelli

University of Parma, Department of Chemistry, Life Sciences and Environmental Sustainability, Parco Area delle Scienze 157/A, 43124 Parma, Italy

ARTICLE INFO

Keywords:
Radiocarbon dating
Landslide events
Atmospheric circulation
Holocene
GIS
Northern apennines

ABSTRACT

In this work we examine the spatial and temporal distribution of radiocarbon dates from landslides on the NE-facing side of the Northern Apennines during the Holocene, focusing on the region's associated vegetation and climatic changes. We also propose a method for identifying areas and landslides that may contain very old organic materials for future research in the region. This analysis was based on a principal component analysis (PCA) on 5255 grid cells measuring 1 km^2 each, overlaid on the study area. These grid cells incorporated variables derived from the terrain characteristics, including underlying lithologies and topographic features.

Our findings reveal that, during the upper Holocene, the last dated events of recurrent and single-event landslides occurred first closer to the coldest and wettest territories once occupied by the glacier termina during the Last Glacial Maximum (LGMgt). Subsequently the last dated events occurred at distances greater than 30 km from the LGMgt, towards the mountain chain's margin. Conversely, at the beginning of the Holocene, an opposite pattern emerged, with landslide events occurring towards the chain interior. These spatial patterns were consistently observed when considering also the entire dataset of 87 dates for landslide events. During the middle Holocene, we observed that the recurrent landslides were primarily concentrated within a narrow belt 8.5 km from the LGMgt. Furthermore, higher rates of landslide activity were associated with the 4.2 ka BP event and persisted until approximately 2.0 ka BP, indicating a correlation with wet and cool periods. In conclusion, these spatial patterns in landslide events can be linked to changes in precipitation patterns and dominant atmospheric circulation in the mountain belt occurred since the beginning of the Holocene.

1. Introduction

1.1. Landslides dating

The dating of landslide events is crucial for reconstructing slope evolution or accurately assessing landslide hazards zonation on a slope or basin scale. However, dating landslide events is a complex task that necessitates selecting the appropriate dating technique, locating suitable yet not always abundant materials, and devising an efficient strategy to identify sites where such materials may be found (Lang et al., 1999). Searching for suitable materials is often time-consuming and frequently dependent on chance rather than the results of a systematic approach.

Excluding anthropogenic influences, under natural conditions, the reactivation or occurrence of a landslide can be influenced to varying degrees by rainfall events. Other reactivations may be more closely associated with unpredictable endogenous forces, such as earthquakes, or with orogenic and tectonic processes linked to mountain formation and relief creation (Korup et al., 2010; Larsen and Montgomery, 2012; Roering, 2012). In a given region, and particularly for certain types of landslides such as debris and mudflows, lateral spreads, rotational and translational slides (with falls or topples being perhaps less affected), ongoing trends in landslide occurrence or reactivation periods can also be correlated with climatic conditions. Numerous studies have established a link between landslide activity and climate (e.g., Corominas and Moya, 2008; Gariano and Guzzetti, 2016), often associating dated events since the Last Glacial Maximum (LGM) with phases of glacier retreat and the presence of a more humid and cooler climate (for Europe, see Borgatti and Soldati, 2002, 2010, and related references). Globally, landslides are particularly associated with glacial-interglacial transitions, and during the Holocene, they are linked to the middle to upper Holocene transition (around 5–4 ka) (Pánek, 2019). Interestingly, Dapples et al. (2002) linked dated landslides to climate, vegetation changes, and anthropogenic activities in the Western Alps. They identified five periods of increased landsliding during the Holocene: 5700–5400,

* Corresponding author.
E-mail address: giovanni.leonelli@unipr.it (G. Leonelli).

https://doi.org/10.1016/j.catena.2023.107705
Received 21 June 2023; Received in revised form 14 November 2023; Accepted 21 November 2023
Available online 30 November 2023

3500–3000, 2800–2300, 1600–1300, and 700–300 cal a BP. Cold and humid climates are also associated with a higher frequency of dated events at several sites in northern Italy, including the Alps and the Northern Apennines (Soldati et al., 2004, 2006). They used a GIS-based approach to characterise site distribution, geographical features, dating techniques, and stratigraphic context, finding higher frequencies of dated events during the Holocene, especially in the 5500–1000 cal a BP period. Furthermore, they associated the altitude of the landslide crown with the age of the event, observing earlier activations (during the lower Holocene) at lower elevations and later activations at higher altitudes in more recent times (upper Holocene).

A recent study on a 13-m-thick sedimentary succession in the peat bog known as 'Lake Moo' in the Northern Apennines revealed clusters of coarse-grained alluvial deposits. These deposits have been associated with extreme paleoflooding events that occurred during the Holocene Thermal Maximum phases and, more recently, coinciding with significant climate change (Segadelli et al., 2020). This recent climate change period is marked not only by well-documented global atmospheric warming (Myhre et al., 2019) but also by the occurrence of extreme precipitation events.

Information regarding landslide reactivations is crucial for land management, and considering the long-term perspective is an essential component of comprehensive hazard assessment. When evaluating landslide occurrences and reactivations over extended periods spanning several centuries and thousands of years, understanding their direct interaction with vegetation becomes paramount. This is because radiocarbon dating of biological remnants found within landslide deposits, such as wood, peat, or organic matter, often serves as the sole source of valuable insights into past landslide activities. In the North-Eastern Apennines, landslide activity is extensively documented in the Parma and Reggio-Emilia districts, where a substantial dataset of up to 95 radiocarbon dates is available (Tellini and Chelli, 2003; Bertolini et al., 2004; Soldati et al., 2006; Bertolini, 2007).

1.2. Study area

1.2.1. Geology and landslides in the Northern Apennines

The study area is in the Northern Apennines of Italy, a mountain chain-oriented NW-SE. It spans approximately 300 km south of the Po Plain and reaches its highest point at Mt. Cimone, 2165 m a.s.l. This area is encompassed within Liguria, Emilia-Romagna, and Tuscany.

Specifically, we selected a portion of the North-Eastern Apennines in the Emilia-Romagna region, which includes the hilly and mountainous districts of Piacenza, Parma, and Reggio-Emilia. This region covers an area of 8324 km^2 of total surface, with 4769 km^2 situated above an elevation of 200 m a.s.l. Within this territory, approximately 30 % of the total area is affected by various types of landslides. Of this, 9 % is characterised by landslides currently classified as active, while 21 % is characterised by inactive or relict landslides, as per the Regione, 2021database.

Most of these landslides consist of large complex earth slides and earth flows, primarily composed of weak rocks such as clayey flysch and mélanges (Bertolini et al., 2017).

The Northern Apennines have evolved as a folded and thrust belt since the Cretaceous period due to the convergence and subsequent continent-to-continent collision between the Adria and Europa plates (Molli, 2008, and references therein). The sedimentary sequences, representing former paleogeographic regions, have been thrust over one another, creating a series of tectonic units distinguished by varying lithological, structural, and tectonic characteristics. These attributes significantly contribute to the predisposing factors for landslides in the region (Bettelli and De Nardo, 2001).

The area comprises rocks with a high clay and claystone content, exhibiting pseudocoherent behaviour. These rocks are interbedded with limestones and sandstones that display a more coherent to semicoherent behaviour within complex rock masses. This contrast in lithology and lithotechnic properties among different rock types is pivotal in promoting slope instability, influenced by factors such as slope angles, structural features, and hydrogeological behaviour.

In the Northern Apennines, the development and distribution of large landslides are closely tied to tectonics, playing dual roles – passive and active. Tectonics act passively by creating lines of weakness and failure surfaces while also actively promoting landslides through topographic growth and the over-steepening of slopes (Carlini et al., 2016).

Additionally, a tectonic and structural approach reveals that translational or rotational landslides in the region are linked to the formation of wide antiforms. These antiforms influence slope angles and the increased incision of watercourses. These effects concern local tectonic discontinuities, sedimentary bed attitude, and lithology (Carlini et al., 2018).

1.2.2. Paleoclimate in the Northern Apennines

Glacial evidence in the study region is apparent through numerous well-preserved landforms and deposits in the mountain chain's inner and upper portions. This concentration is particularly notable in the southeastern part of the region, where the highest peaks rise, with only a few exceeding 2000 m a.s.l. (Fig. 1; Bettelli et al., 1982; Federici and Tellini, 1983; Chelli and Tellini, 2002; Giraudi, 2004, 2011; Baroni et al., 2018).

The Late Pleistocene glacial cycles in the Apennines reached their climax during the Last Glacial Maximum (LGM), occurring approximately between 30 and 16 cal ka BP (Giraudi and Frezzotti, 1997; Giraudi, 2004). During this period in the Northern Apennines, more than 100 valley and mountain glaciers were widespread, particularly in the north-facing sector, encompassing the Parma and Reggio-Emilia districts. The local LGM dates back to periods before 21 ka (Baroni et al., 2018). Subsequently, all glaciers vanished from the Northern Apennines before the onset of the Younger Dryas (Hughes and Woodward, 2008; Giraudi, 2004).

Numerous climatic insights can be gleaned from pollen stratigraphic analyses of lake sediments or peat bogs. These analyses often enable a continuous reconstruction of past climates by studying vegetational changes. During the LGM, cold and arid conditions predominantly favoured steppe and tundra environments across northern Eurasia, displacing forest biomes southward (Prentice et al., 2000). This shift extended as far as the circum-Mediterranean area, which served as a refuge for broadleaf species. Steppe environments characterised Southern Europe (Elenga et al., 2000), and loess deposition occurred in the Po Plain (Cremaschi, 1990).

Following the LGM and up to the Late Glacial interstadial warming around 14.7–14.5 cal ka BP) the Apennine foothills bordering the Po Plain featured *Pinus sylvestris-Betula* woodlands. Meanwhile, spruce (*Picea abies* (L.) Karsten), an indicator of continental dryness, expanded primarily in the inner Apennine region (Lagdei and Berceto sites; Bertoldi, 1981; Bertoldi et al., 2004; Lowe, 1992; Lowe and Watson, 1993) and particularly in the Alps (Ravazzi, 2002).

The decline of spruce in the Northern Apennines commenced during the Late Glacial interstadial (Lowe, 1992), with an earlier onset in the western sector and a later start, at the beginning of the Holocene, in the eastern sector (Lake Greppo). This transition saw the replacement of spruce by fir (*Abies alba* Mill.), a species adapted to moist climatic conditions (Ravazzi et al., 2006). The delayed advance of *Abies*, even up to the treeline, can be attributed to the dry conditions prevailing on the Adriatic eastern side of the Apennines during the Late Glacial period. Additionally, this region was farther from the Adriatic Sea during the Late Glacial period (Lambeck et al., 2004) than today, owing to a lower sea level of approximately 90 m. Indeed, in the Northern Apennines, the absence of sediments dating to the Late Glacial and Early Holocene has been interpreted as a consequence of dry climatic conditions (Ponel and Lowe, 1992; Lowe and Watson, 1993).

The warming during the Early Holocene occurred rapidly and was accompanied by heightened moisture conditions in the eastern sector of

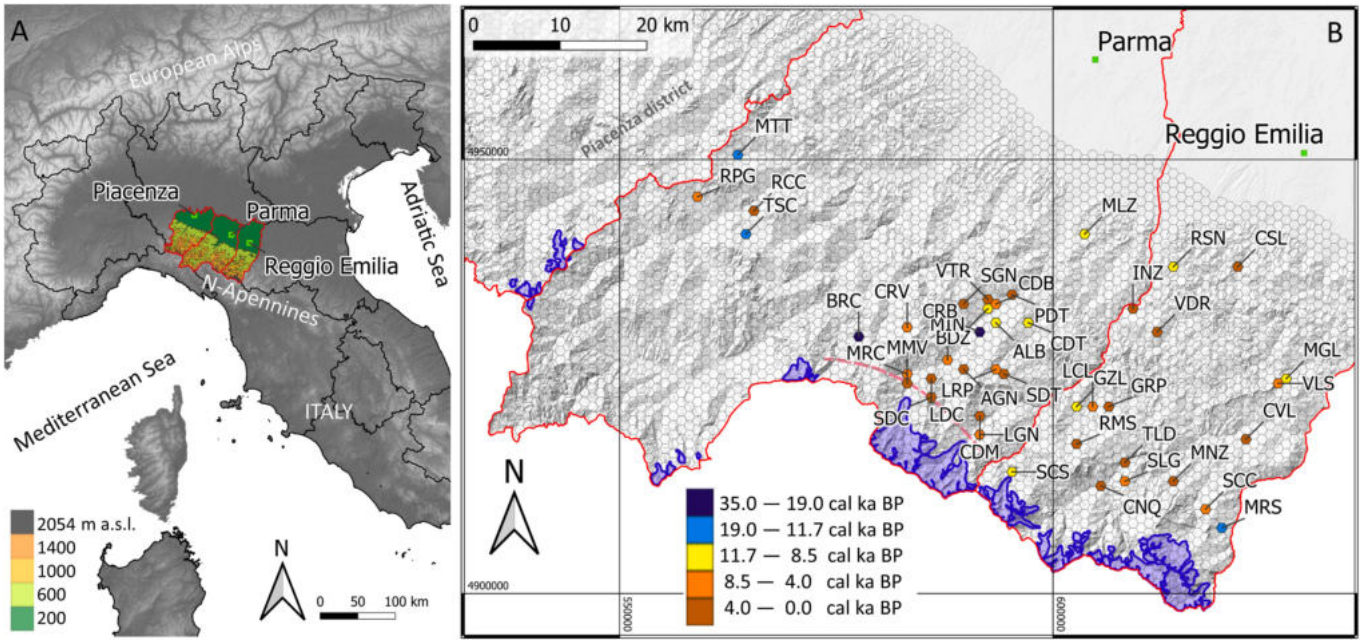

Fig. 1. Location of the study area in the Northern Apennines, Italy (A), included the districts of Piacenza, Parma and Reggio-Emilia, comprising only a small portion of the Po Plain, the hills and the mountains up to the mountain divide located in the south-west. Distribution of the dated landslides included in the superimposed hexagon grid of 1 km^2 cells (B): cells are coloured according to the oldest date obtained from radiocarbon dating at each landslide. For the landslide names and details, see the corresponding acronyms reported in Table 1. The figure also depicts the extension of the glaciers during the LGM (in blue; Baroni et al., 2018) and an antiform structure located in the southern portion of the area (dashed red line) (Carlini et al., 2018). (For interpretation of the references to colour in this figure legend, the reader is referred to the web version of this article.)

the Northern Apennines. This shift is evident through the swift establishment of a continuous forest cover, primarily dominated by *Abies*, and subsequently, especially at lower altitudes, by *Quercus*, *Acer*, *Fraxinus*, *Tilia*, and *Ulmus* (from approximately 10,400–8000 to 5000 a BP; Watson, 1996). The transition in vegetation should be viewed as a spatial phenomenon across the region, with changes commencing earlier at lower elevations and progressively reaching the highest elevations of the treeline. In periods likely associated with the lower and middle Holocene, which includes the climatic optimum, it is worth noting that at the Mt. Cusna site (located a few kilometres southeast of the study region), the forest cover reached altitudes of up to 1850 m. This was approximately 100 m higher than the current treeline, as indicated by buried paleosols (Compostella et al., 2014). Pollen sequences spanning the last 30000 years, extracted from the Berceto and Lagdei lacustrine deposits, provide insight into the Holocene period. Mixed forests of *Abies* and *Quercus* characterised the landscape during its early phase. The arrival of *Fagus*, however, occurred 6800 a BP (Bertoldi et al., 2007) and reached its maximum distribution in the Northern Apennines around 5000 a BP (Lowe, 1992).

1.3. Research objectives

Radiocarbon dates obtained from landslides are typically closely linked to the particular landslide where organic materials were discovered and to the type and movement of the landslide. When considering a broader region, these dates are often presented regarding their geographical distribution and chronological evolution concerning climate changes. However, they typically lack a clear spatial and temporal correlation with climate and a quantitative assessment of the geographical features such as topography and the primary underlying lithology. These geographical features are essential for understanding the preservation of materials suitable for dating purposes.

The primary objective of this paper is to examine regional-scale spatial patterns of landslide events that occurred during the Holocene, which encompasses the period with the highest number of available radiocarbon dates. This analysis aims to establish connections between the timing of these landslides and climatic condition changes. Additionally, we seek to investigate the relationships between the dated landslide events in the realized database and various geographical factors that influence the preservation of datable materials. These factors include lithology and the lithotechnic behaviour of rocks, geomorphology, and topography. We aim to develop a systematic approach to pinpoint areas where landslide bodies may contain organic material suitable for dating landslides and extracting valuable climatic information from older remnants.

In the course of our research, we also evaluate whether the radiocarbon dates of landslide events, collected over decades of research conducted in the North-Eastern Apennines (Tellini and Chelli, 2003; Bertolini et al., 2004; Soldati et al., 2006; Bertolini, 2007), are evenly distributed across various geographical features, such as topography, lithology, slope angle, elevation, and landslide type. Alternatively, we assess whether certain parts of the region are over- or under-represented in the dataset due to the influence of these territorial features, which may also impact the preservation of organic datable material.

2. Methods

2.1. GIS project and radiocarbon dates

A GIS project was established using the QGIS (2022) software (version 3.16) to create a spatial database of available dates from landslides. This database also included a grid of 1 km^2 hexagonal cells superimposed over the entire study area, which spans from 200 m a.s.l. (at the borders of the Po Plain) to the highest point in the south-west, reaching a maximum elevation of 2054 m a.s.l. (Fig. 1). The choice of hexagonal grid cells over square ones was made because of their more rounded shape, which better suited the terrain's coverage.

Along the study region's borders, the grid cells were trimmed to a smaller extent, retaining only those larger than 0.8 km2 within the project. Numerous variables were derived from these cells, including the

predominant underlying lithology (Table 2), surface cover, the primary landslide type, and the overall extent of landslide coverage. Additionally, various topographic variables were derived from a 5-m Digital Elevation Model obtained from Regione Emilia-Romagna (2020). These topographic variables included elevation, slope, plane and tangential curvature, and roughness and were assessed for their mean, maximum, minimum, and range values within each grid cell.

Supplementary information, such as the landslide code reported in the Landslide Inventory Map and Landslides Historical Archive (Regione Emilia-Romagna, 2021) and the IFFI code (ISPRA, 2021), was also integrated into the project.

Ninety-five radiocarbon dates, obtained from 43 landslides within

Table 1
Landslides names and types of radiocarbon-dated materials, as well as main characteristics of the 1 km^2 grid-hexagon cells where the 43 dated landslides are located. Data are ordered, separating the recurrent landslides (23) from those presenting only one dated organic sample (20) and according to a decreasing distance from the LGM glacier terminus. PC, PR, and RE are acronyms for the Piacenza, Parma and Reggio-Emilia districts. Type of radiocarbon-dated material (total of 95 dates): (WR) wood remains, (T) trunk, (OM) organic matter, (B) organic matter from a borehole, NA not available information. For the acronyms of * Main landslide type and ** Main lithology in the cells, the reader is referred to Tables 2 and 3, respectively. ^{14}C ages are from Tellini and Chelli (2003), Bertolini et al., (2004; 2005), Bertolini (2007).

Landslide toponym	Landslide acronym	Administrative district	No. ^{14}C dated samples	^{14}C Age of oldest sample (yr. BP)	Type of dated material	Main landslide type in grid cell *	Main lithology in grid cell **	Mean elevation of grid cell (m s.l. m.)	Grid cell distance from LGM glacier terminus (km)
Marra Molino Vecchio	MMV	PR	2	3290 ± 60	(WR)	a2g	Dm	713	1.1
Lugagnano	LGN	PR	2	6000 ± 50	NA	a2h	Dsc	815	1.3
Marra Centrale	MRC	PR	3	4460 ± 50	(WR)	a2g	Dsc	710	2.2
La Lama-Corniglio	LDC	PR	3	1550 ± 50	(WR)	a1g	Blp	754	2.9
Secchio	SCC	RE	3	5310 ± 70	(WR)	a2g	Dsc	845	3.7
Morsiano	MRS	RE	2	11390 ± 70	(T)	a2g	Dsc	812	3.8
Miano	MIN	PR	3	3940 ± 60	(WR)(B)	a2g	Bp	563	5.7
Berceto Spz2-2	BRC	PR	4	29620 ± 290	(OM)(B)	a2h	Bp	650	5.9
Cerrè Sologno	SLG	RE	6	4510 ± 40	(WR)(B)	a1g	Dsc	822	7
C.Cozzo = M. Cervellino	CRV	PR	9	5730 ± 50	(WR)	a1d	Blp	1078	7.5
Le Ripe (Schia)	LRP	PR	2	5360 ± 60	(WR)	a2g	Blp	1121	8.5
Talada	TLD	RE	2	2530 ± 60	(WR)(B)	a2g	Gc	551	8.8
Carobbio	CRB	PR	3	25129 ± 160	(WR)(B)	a2g	Blp	608	10.6
Gazzolo	GZL	RE	5	8090 ± 70	(WR)(B)	a1g	Dsc	638	10.6
Cavola	CVL	RE	5	3660 ± 40	(WR)(B)	a2g	Bp	480	13
Beduzzo	BDZ	PR	2	7810 ± 50	(WR)	a2g	Blp	498	13.2
Groppo	GRP	RE	2	1980 ± 60	(OM)(B)	a1g	Dsc	582	13.4
Riopoggione	RPG	PR	2	3880 ± 60	(WR)	a2g	Dol	709	13.8
Tosca	TSC	PR	4	12120 ± 50	(WR)(B)	a1g	Bp	598	15
Rocca	RCC	PR	3	2580 ± 60	NA	a2g	Blp	543	17.2
Metti Bh	MTT	PR	3	10230 ± 80	(WR)	a2g	Bp	562	20.1
Ienza	INZ	RE	3	1540 ± 40	NA	a2g	Dsc	318	23.4
Casoletta	CSL	RE	2	580 ± 40	(WR)(B)	a1d	Dsc	271	31.2
Succiso	SCS	RE	1	8380 ± 60	(T)	a1b	Dsc	863	0
Sivizzo di Corniglio	SDC	PR	1	100 ± 0.5	(WR)	a1h	Blp	1086	1.9
Casanova di Monchio	CDM	PR	1	3350 ± 60	(WR)	a2g	Bp	809	2.8
Cinquecerri	CNQ	RE	1	3620 ± 60	(T)	a2d	Dsc	598	5.4
Minozzo	MNZ	RE	1	960 ± 40	(WR)(B)	a2g	Blp	709	5.5
Agna	AGN	PR	1	2820 ± 60	(WR)(B)	a2h	Blp	904	6.6
Ramiseto	RMS	RE	1	2930 ± 40	NA	a2g	Dsc	1058	7.9
Schia di Tizzano	SDT	PR	1	420 ± 40	(WR)	a2h	Blp	1164	8.4
Lucola	LCL	RE	1	4380 ± 60	(T)	a2g	Dsc	500	11.9
Signatico	SGN	PR	1	120 ± 40	NA	a1b	Bl	891	11.9
Albareto 1	ALB	PR	1	8090 ± 60	(WR)	a2g	Blp	563	12.8
Molino Vecchio Tre Rii	VTR	PR	1	1500 ± 50	(WR)	a2g	Blp	584	14
Costa di Beduzzo	CDB	PR	1	5400 ± 50	(WR)(B)	a2g	Blp	454	14.2
Cozzo di Tizzano	CDT	PR	1	8280 ± 70	(WR)(B)	a2g	Blp	591	14.9
Porcelloso di Tizzano	PDT	PR	1	100 ± 0.6	(WR)	a2g	Blp	405	16.3
Valestra	VLS	RE	1	3980 ± 60	(OM)(B)	a1h	Bl	669	20.5
Magliatica	MGL	RE	1	9190 ± 60	NA	a1g	Dol	491	21.4
Vedriano	VDR	RE	1	119 ± 0.8	NA	a2g	Dsc	601	22.7
Mulazzano 1	MLZ	PR	1	9960 ± 70	(WR)	a2g	Bl	314	27
Rossena 4	RSN	RE	1	8960 ± 60	(OM)(B)	a1g	Dsc	342	30.1

the study area (Table 1), underwent calibration using Calib software (version 8.2; Stuiver et al., 2022) and the IntCal20 Northern Hemisphere radiocarbon age calibration curve (Reimer et al., 2020). Calibrated dates associated with organic remains, including wood fragments, trunks, and organic matter, were integrated into the GIS project, each linked to its respective landslide of origin.

To ascertain the most likely calibrated date, we followed our regional-scale approach. For each calibrated date accompanied by 2σ ranges (often encompassing multiple time intervals), we selected a single date as follows: the mean date from the sole interval that exhibited a relative area under the probability distribution ≥ 0.6 or the mean date derived from all intervals with a relative area under the probability distribution < 0.6.

The dates were analysed temporally and spatially, considering various environmental variables. These variables included the distance between the hexagonal grid cell containing the main, lower, portion of a dated landslide and the closest Last Glacial Maximum glacier terminus (LGMgt, in this study, treated as a variable combining information from regions representing the coldest and wettest areas), the distance from the primary mountain divide located in the south-west of the study area, and the elevation of the cell. To determine the position of the LGMgt, we referred to Baroni et al. (2018) and their cited sources. All measurements of distances and elevations were conducted within the GIS project.

2.2. Landslides and territorial features

To identify potential spatial patterns in dated landslides concerning geo-lithological and topographic factors, a principal component analysis (PCA) was conducted. The original matrix was structured with grid cells in rows and normalised variables in columns. This PCA was executed using PAST4 software (Hammer et al., 2001), encompassing indexed variables associated with various lithologies present in each grid cell and the topographic attributes of these cells across the three selected districts of Piacenza, Parma, and Reggio-Emilia.

Within the geo-lithological variables employed, the Geological Strength Index (GSI), which ranges from 0 to 100 (Hoek and Brown, 1997; Marinos et al., 2005), was calculated for each rock type in the region. To use rock strength as an indicator of rock resistance to gravitational processes and debris production, we adopted mean GSI values derived from typical GSI ranges for various rock types, following the guidelines of Marinos and Hoek (2000). These rock types included sandstone, siltstone, claystone, clay shale, limestone, granite, ophiolite, gneiss, schist, and flysch (Mandrone, 2004) (Table 3). GSI values were unavailable for gypsum, so we categorised massive and stratified gypsum as As and Cc groups, respectively (Table 3). Rock types were grouped according to mass lithotechnic characteristics following the clustering scheme proposed by Regione Emilia-Romagna (2021), and mean GSI values were computed for each group (Table 3). Additionally, for massive rocks (A), we incorporated the theoretical GSI range values for intact to blocky rocks. Another complex variable was introduced, referred to as 'GWI × Mean Slope': Geological Weakness Index (GWI; ranging from 100 to 0, being calculated as the reciprocal of the mean GSI) multiplied by the mean slope angle.

Among the topographic variables considered, after conducting multiple PCA runs, we retained only the range of profile and tangential curvature and the mean roughness, as they better elucidated the dataset's variability.

Considering the potential significance of very old organic material for paleoclimatic reconstructions, our attention shifted to two landslides that yielded remnants dating back to periods preceding the LGM, namely the Berceto and Carobbio landslides. Within the 2D space of the PCA analysis, we identified the ten closest grid cells for both landslides. These grid cells represented the regions most closely aligned with the lithological and topographic characteristics of the two landslides. Further refinement was performed by selecting cells situated at similar altitudes to the two landslides (above 600 m a.s.l.) and exhibiting the same landslide type. This allowed us to identify counterparts to the two recognised oldest landslides in the study area in terms of territorial features possibly promoting the conservation of datable materials.

Table 2
Acronyms were used to classify landslide deposits in the Regione Emilia-Romagna (2021) and adopted in this study.

		a0	Undetermined stabilized or relict landslide deposit
a1	Undetermined active landslide deposit	a2	Undetermined dormant landslide deposit
a1g	Complex active landslide deposit	a2g	Complex dormant landslide deposit
a1a	Fall or topple active landslide deposit		
a1b	Rotational or translational active landslide deposit	a2b	Rotational or translational dormant landslide deposit
a1h	Massive rotational or translational active landslide deposit or Deep-seated gravitational slope deformation	a2h	Massive rotational or translational dormant landslide deposit or Deep-seated gravitational slope deformation
a1d	Mud flow active landslide deposit	a2d	Mud flow dormant landslide deposit
a1e	Debris flow active landslide deposit	a2e	Debris flow dormant landslide deposit

2.3. Comparisons with other reconstructions and vegetation changes

To illustrate temperature variations during the Holocene in our study area, we incorporated the Holocene July temperature reconstruction from the Western Alps' Rutor Glacier region (at an altitude of 2510 m a.s.l.), as presented by Badino et al. in 2018, relying on pollen data. This analysis was conducted due to the substantial correlation, denoted by Pearson's $r = 0.98$, established between contemporary July temperature data obtained from grid data (CRU TS Version: 4.06; Harris et al., 2020) originating in the Western Alps (specifically, the grid cell encompassing the Rutor area at Latitude 45.75° N and Longitude 6.75° E, with a mean elevation of 1923 m a.s.l.) and the grid cells covering our study area within the Northern Apennines (Latitude 44.75° N; Longitude 9.25° E, Latitude 44.75° N; Longitude 9.75° E, Latitude 44.75° N; Longitude 10.25° E, Latitude 44.25° N; Longitude 9.75° E, and Latitude 44.25° N; Longitude 10.25° E, with a mean elevation of 552 m a.s.l.).

To align the temperature series from the Rutor area with the Western Alps' grid cell's mean elevation, we applied a stepwise transformation, accounting for a lapse rate of 6 °C per 1000 m. Subsequently, we adjusted the temperature series to align with the elevation of the grid cells in our study area using a regression equation that links July temperatures in the two regions mentioned above. Ultimately, we determined the elevation of the July 13 °C temperature isotherm throughout the Holocene for the Northern Apennines. This isotherm bears significant relevance as it is a critical indicator for the northern extent of forests within the boreal zone (L'Abée-Lund et al., 2009; L'Abée-Lund et al., 2021). Furthermore, it constitutes a recognised limiting factor for the prevailing forest type found at the highest altitudes within the Northern Apennines, namely the European beech (*Fagus sylvatica* L.) forest (Pezzi et al., 2008).

To illustrate precipitation variations over the study region during the Late Glacial period and the Holocene, we relied on the PaleoView model (Fordham et al., 2017), a tool for extracting high-resolution climatic data, globally, for any period during the last 21000 years.

3. Results

3.1. Landslide characteristics and time distribution

The hexagonal grid encompasses 5255 cells that span the Piacenza,

Table 3
Acronyms for rock masses (adopted as in the Topographic Database of the Regione Emilia-Romagna, 2020), general lithotechnic characteristics of rock masses, and mean Geological Strength Index GSI value derived from the expected GSI range of the associated rock types (Marinos and Hoek, 2000). Table numbers in the 'Rock type' column and the number associated with a rock type refer to Marinos and Hoek (2000).

Rock masses acronym	Rock masses lithotechnic characteristics	Rock type	min GSI	max GSI	mean GSI	st. dev.
A	Massive rocks	Granite (table 8)	49	91	69.3	25.6
		Ophiolite 1 (fresh; table 9)	37	87		
		Limestone 1 (massive; table 7)	43	92		
		Intact to blocky rocks (general scheme)	55	100		
As	Stratified rocks	Sandstone 1 (massive or bedded; table 5)	42	95	68.0	29.5
		Limestone (massive; table 7)	43	92		
G	Massive or stratified gypsum		–	–		
Bl	Structurally ordered rock masses with alternations of stone levels (Ex: cemented sandstones, calcarenites, calcilutites, etc.) and pelitic levels; prevailing stone levels: L/P > 3	Flysch A (table 12)	43	74	57.5	23.2
		Sandstone 1 (massive or bedded; table 5)	42	95		
		Limestone 2 (thin bedded; table 7)	34	57		
Blp	Structurally ordered rock masses with alternations of stone levels (Ex: cemented sandstones, calcarenites, calcilutites, etc.) and pelitic levels; 1/3 < L/P < 3	Flysch B, C, D, E (table 12)	28	53	51.5	24.0
		Sandstone 1 (massive or bedded; table 5)	42	95		
		Limestone 2 (thin bedded; table 7)	34	57		
Da	Stratified clays, marly clays and silty clays	Claystone, siltstone 1 (bedded, foliated, fractured; table 6)	21	44	32.5	16.3
Cc	Clasto-supported conglomerates and breccias with medium to low cementation	Sandstone 2 (brecciated; table 5)	27	44	26.0	14.6
		Claystone 2 (sheared, brecciated; table 6)	5	26		
		Ophiolite 2 (serpentinised with brecciation and shears; table 9)	7	26		
		Limestone 3 (brecciated; table 7)	28	45		
Gc	Chaotic gypsum		–	–		
Cs	Lightly cemented sandstones and arenites	Ophiolite 2 (serpentinised with brecciation and shears; table 9)	7	26	26.0	15.1
		Sandstone 2 (brecciated; table 5)	27	44		
Bp	Structurally ordered rock masses with alternations of stone levels (Ex: cemented sandstones, calcarenites, calcilutites, etc.) and pelitic levels; prevailing pelitic levels: L/P < 1/3	Flysch F (table 12)	10	30	24.3	18.6
		Schist 1, 2 (strong and weak; table 11)	15	58		
		Schist 3 (sheared; table 11)	8	25		
Dm	Marl	Claystone, siltstone 1 (bedded, foliated, fractured; table 6)	21	44	24.0	16.1
		Claystone, siltstone 2 (sheared, brecciated; table 6)	5	26		
Dol	Clay breccias with chaotic primary structure (debris flow and mud flow)	Flysch G, H (table 12)	4	28	16.3	12.5
		Ophiolite 2 (serpentinised with brecciation and shears; table 9)	7	26		
Dsc	Clay shales, intensely tectonized	Claystone 2 (sheared, brecciated; table 6)	5	26	15.5	14.8

Parma, and Reggio-Emilia districts. These cells have been characterised based on various topographic and geological variables, as well as the presence of dated landslides (Fig. 1). Among these cells, most of the 43 containing dated landslides are located in the Parma district (25), followed by Reggio-Emilia (18), while there are currently no available dates for the Piacenza district.

The 95 radiocarbon dates correspond to cells that either exhibit recurrent landslides (23; mean elevation 663 m a.s.l.) or those with only one recorded date (20; mean elevation 680 m a.s.l.) (Table 1). The predominant type of dated landslide within the dated grid cells is the

complex landslide, totalling 32 landslides, of which seven are classified as active (codes in Table 2: a1g and a2g). This is followed by the massive rotational or translational landslide, with a total of six, two of which are classified as active (a1h and a2h), the mud flow landslide (three, with two classified as active; a1d and a2d), and rotational or translational landslides (two active landslides; a1b). Radiocarbon dates are not associated with cells that fall or topple landslides (a1a) dominate surface cover or where debris flows (a1e and a2e) are present.

In summary, the majority of the dated landslides are located in areas where flysch formations predominate (24 landslides; Bl = 3; Blp = 15; Bp = 6; see Table 3 for lithology acronyms) or where intensely tectonised clay shales dominate the cells (15 landslides; Dsc). Other lithologies include clay breccias (two landslides; Dol), marl (one; Dm), and chaotic gypsum (one; Gc). Notably, the oldest-dated landslides, namely the Berceto (29620 ± 290 years BP) and the Carobbio (25129 ± 160 years BP) landslides, are located in areas where the flysch of Scabiazza sandstone (Bp) and the flysch of Monte Caio (Blp) formation predominate, respectively (Table 1).

The analysis of the temporal distribution of the 95 dated samples in the study area reveals that only eight samples are associated with periods before the Holocene. Specifically, three samples date back to periods preceding the LGM, and five are linked to the Late Glacial period (Fig. 2).

Most of the dates (87, accounting for 91.6 % of the total available dates) belong to the Holocene epoch, primarily within the recent period up to 3.5 cal ka BP. Within this Holocene category, 51 samples (53.7 %) are concentrated, with the highest concentration occurring in the 3.0–2.5 cal ka BP timeframe, consisting of 13 samples.

3.2. *Spatial patterns in landslide and variable selection: The last dated events*

After segregating landslides into two categories based on the number of dated occurrences – those with multiple dates (23 recurrent landslides) and those with only a single date (20 single-dated landslides) – and initially considering solely the last, most recent, calibrated date from each landslide, we identified spatial patterns of events across the study area (Fig. 3). The most recent calibrated ages exhibited correlations with the distance from the locations once occupied by the LGM glacier termina (LGMgt Fig. 3A and 3B), as well as proximity to the nearest main mountain divide in the south-west of the study region (Fig. 3C and 3D).

Regression analysis indicates that the recurrent landslides experienced their last significant events, including organic materials, at approximately 3 cal ka BP and were situated nearby (approximately 3 km) to the LGMgt. Subsequently, more recent events occurred at increasing distances from the LGMgt (Fig. 3A). The linear regression of age over distances yields an adjusted determination coefficient R^2_{adj} = 0.37. One recurrent landslide, the Beduzzo landslide, was excluded from the regression analysis due to an out-of-range value for the most recent recorded event. This group of recurrent landslides encompasses those that were active both in the pre-LGM and Late Glacial periods and throughout the entire Holocene.

The landslides associated with a single-dated event exclusively occurred during the Holocene period (Fig. 3B). Landslides dating back to the middle and upper Holocene exhibit similar spatial patterns to the most recent events of the recurrent landslides. Those landslides positioned closer to the locations once occupied by the glacier terminus experienced earlier events than those at greater distances.

For the landslides occurring in the upper Holocene, the linear regression model indicates a value of approximately 2 cal ka BP at distances of less than 2 km from the LGMgt. The middle and upper Holocene groups demonstrate linear models with the same slope as the last events of the recurrent landslides. However, they have lower determination coefficients due to the greater spread of values (upper Holocene; R^2_{adj} = 0.16) and a lower number of cases (middle Holocene; $R^2_{adj} < 0$).

In contrast to the recurrent landslides and the landslides that occurred in the middle and upper Holocene, those landslides that activated once during the lower Holocene (or more precisely, those that recorded an event involving organic materials) display contrasting spatial patterns (Fig. 3B, yellow points). In this group, landslides occurred earlier at greater distances from the locations once occupied by the LGMgt. At approximately 30 km, events took place at approximately 11 cal ka BP, while at distances of less than 2 km, events occurred at 9 cal ka BP (e.g., Succiso landslide). The regression slope indicates a determination coefficient value of R^2_{adj} = 0.31.

We can make similar observations for recurrent and single-event landslides when examining the distance from the southwestern divide of the mountain chain. However, it's worth noting that for recurrent landslides, there is a greater dispersion of values along the regression line compared to when considering the distance from the LGMgt, resulting in a lower determination coefficient (R^2_{adj} = 0.26; Fig. 3C).

In general, the determination coefficients and slopes of the regression lines exhibit comparable magnitudes across all subgroups, albeit with slightly more variability and a broader range of values when considering the mountain divide.

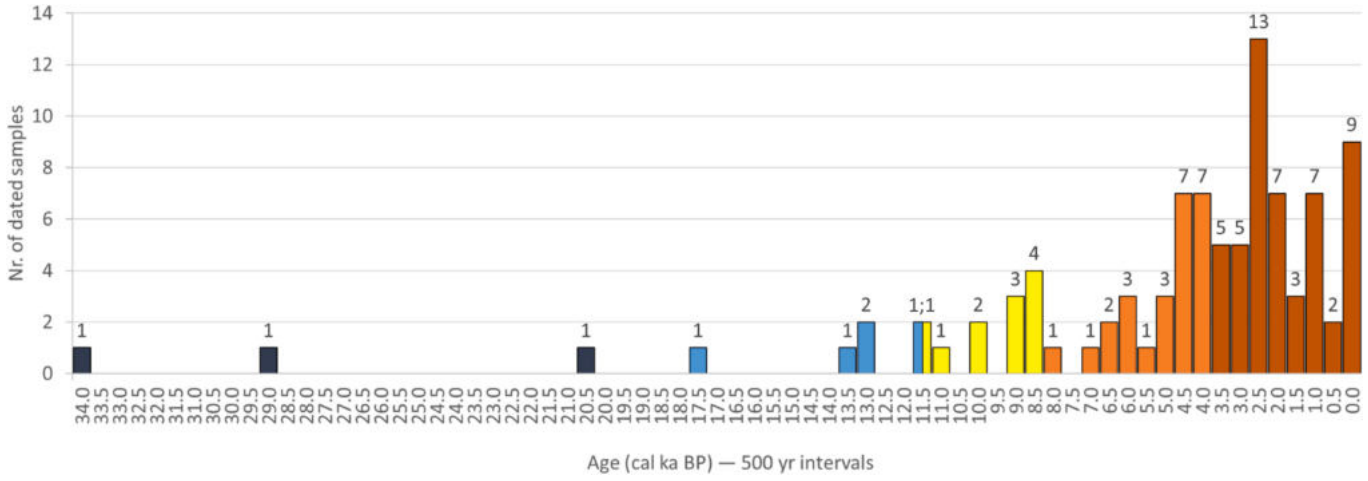

Fig. 2. Time distribution of the 95 dated samples from 43 landslides in the study area. The means of calibrated ages in the figure are grouped every 500 years. Colours are selected as follows: dark blue, before LGM (before 19.0 ka BP); blue, Late Glacial (19.0–11.7 ka BP); yellow, lower Holocene (11.7–8.2 ka BP); orange, middle Holocene (8.2–4.2 ka BP); upper Holocene (4.2–present). For the Holocene subdivisions, we referred to global, abrupt climatic events (Walker et al., 2019). (For interpretation of the references to colour in this figure legend, the reader is referred to the web version of this article.)

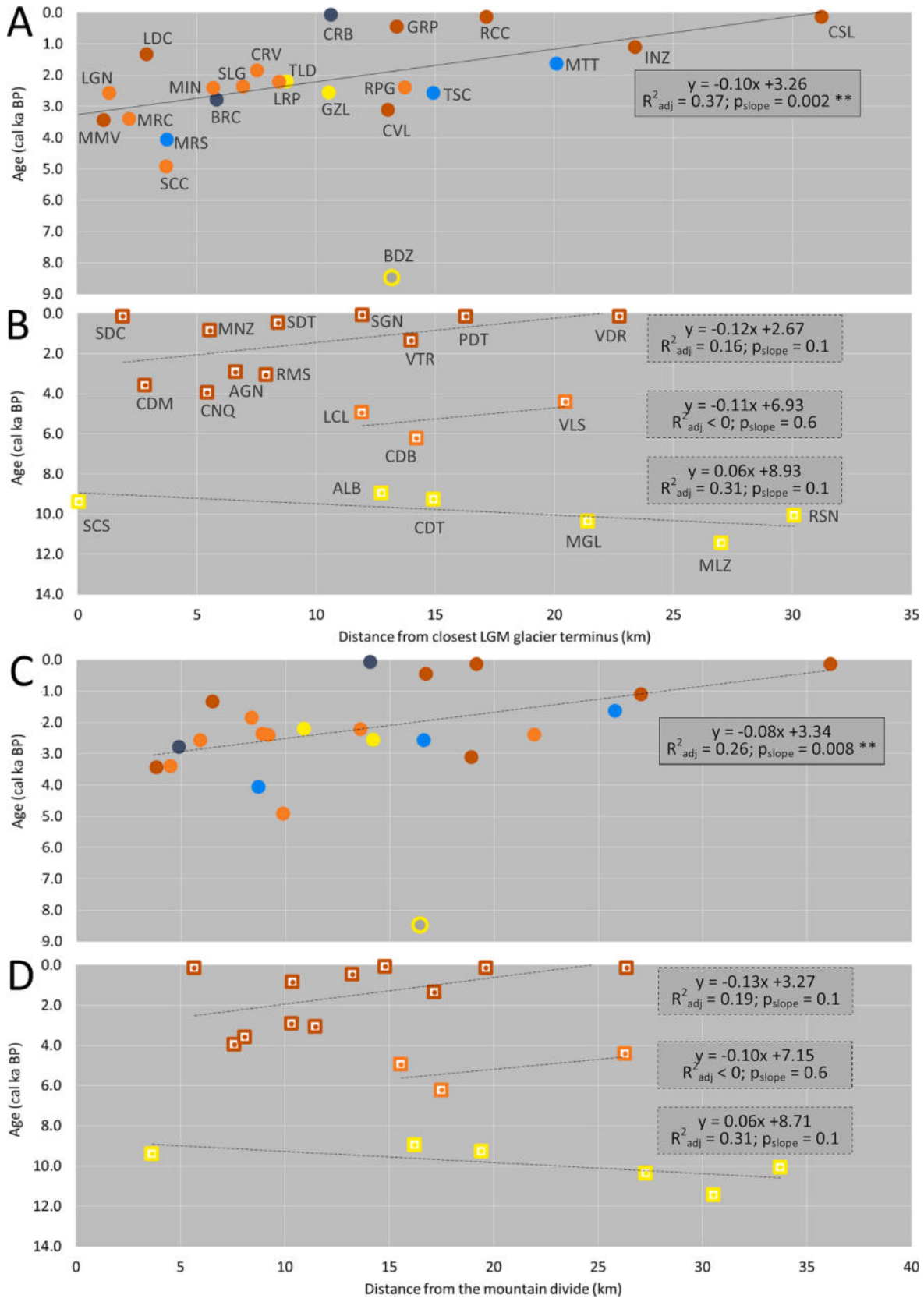

Fig. 3. Regression of the last (most recent) calibrated age obtained from a landslide over the distance of the grid cell, containing the landslide from the closest LGM glacier terminus (A, B) or the closest main mountain divide in the south-west of the study region (C, D). In both cases, the recurrent landslides, i.e., with more than one date (A, C), are separated from the landslides presenting only one date (B, D), and regression lines report the respective equations and determination coefficients. The Beduzzo landslide (BDZ, hollow point) has been excluded from the regression in A and C. All the points representing a landslide are coloured according to the oldest age obtained from the landslide using the same colours as in Fig. 1B; acronyms and landslide details are explained in Table 1.

Lastly, we conducted a similar analysis focusing on the most recent recorded events, examining the age of the dated event concerning two variables: the mean elevation of the grid cell containing a dated landslide (Fig. 4A) and the composite variable that encapsulates the lithological and topographic characteristics of the grid cell (the GWI × Mean Slope variable, as detailed in the Methods section) (Fig. 4B). The last events of recurrent landslides tended to occur initially at higher elevations and subsequently at lower elevations during the middle to upper Holocene. There is no discernible elevation pattern in single-event landslides in the upper Holocene. However, for landslides in the lower Holocene, events were initially recorded at lower altitudes and then at higher altitudes (Fig. 4B). When considering the lithotechnic-topographic variable, we observe that during the upper Holocene, both recurrent (Fig. 4C) and single-(dated) event landslides (Fig. 4D) first occurred in grid cells characterised by steeper slopes and weaker lithologies, followed by occurrences in cells with contrasting characteristics. Such patterns are not evident in landslides occurring during the lower Holocene.

3.3. Territorial features of the grid cells containing dated remnants from landslides

The PCA indicates that the cells, distinguished by lithology, are horizontally distributed primarily parallel to PC1, and separated along PC2 into two main groups, one above and one below PC1 (Fig. 5). The component loadings (Fig. 6) reveal that the variables associated with PC1 are tangential curvature and roughness, accounting for 58.8 % of the total variance. Conversely, along PC2, the significance of the GSI and of the GWI associated with slope dominates, explaining 25.7 % of the total variance. While the PC2 is not fully significant in its range of variability, the two axes of the PCA collectively explain up to 84 % of the total variance in the dataset. Above the PC1 (and along the positive values of PC2), cells present dominant lithologies that are mainly related to GSI alone: massive and stratified rocks (A, As); flysch (Blp, Bl). Below the PC1, cells present lithologies that are mainly related to GWI and mean slope: clay shales (Dsc); lightly cemented sandstones and arenites (Cs); stratified clays and marls (Da, Dm).

An uneven distribution of dated landslides becomes apparent, as no dates of past landslide events are available in areas where certain lithologies dominate in terms of surface cover. Similarly, there are no dated landslides where the topographic surface, including roughness, curvature, and slope, exceeds a central range of values and assumes extreme values (Fig. 5). Regarding the primary dominant lithologies (those dominating in at least 5 % of the total cells, as indicated in the first column of the legend in Fig. 5), it's noteworthy that no dated landslide events are found in areas where lightly cemented sandstones and arenites (Cs in Table 3) predominate in the cell surface. This lithology accounts for 9.2 % of the total cells analysed and ranks fifth in surface outcropping in the study area. It is primarily associated with low roughness, curvature, and slope surfaces, although it does exhibit variation in mid-GSI values.

Concerning the total number of cells containing a specific lithology, the cells characterised by intensely tectonised clay shales (Dsc in Table 3) exhibit the highest percentage of dated landslides, with a rate of 21.1 ‰. In contrast, cells with other dominant lithologies where dated landslides are present typically have rates of 10 ‰ or lower, down to 5.3 ‰ in cases of structurally ordered rock masses with alternating levels, where flysch A types with prevailing stone levels (L/P > 3), including sandstone and limestones (Bl in Table 3), are prominent.

The primary lithology in the area corresponds to the flysch formation with alternating stone levels and pelitic levels, falling within the range $1/3 < L/P < 3$, as well as sandstones and limestones (Blp in Table 3). The PCA analysis reveals no dated landslides are recorded for PC1 values below −2 or above 2, except for a single landslide found at approximately PC1 = 6 (the Succiso landslide). This implies that no dated landslides are associated with cells featuring extremely low or high roughness and curvature range values.

Additionally, no dated landslides for PC2 values exceeding 1.5 correspond to cells with massive rocks and stratified rocks (A and As in Table 3) exposed, along with a rough surface and steep slopes. Conversely, low GSI values and gentle slopes in cells are primarily associated with rock masses characterised by intensely tectonised clay shales (Dsc), representing the group with the highest rate of dated landslides overall. Regarding landslide activity, the two main groups represent recurrent and single-event landslides.

In our search for analogous conditions within the study area, our focus turned to the characteristics of the two grid cells housing the landslides that yielded the oldest-dated organic materials: the Berceto landslide (with organic matter from a borehole) and the Carobbio landslide (featuring wood remnants from a borehole) (Table 1; Fig. 7A).

The ten analogous cells for the Berceto landslide are situated on Bp lithology and are exclusively found within the Parma district. Conversely, the ten cells analogous to the Carobbio landslides are located on Blp lithology and span both the Piacenza and Parma districts. Further refinement was made by selecting the first 20 grid cells that met criteria such as elevations higher than 600 m a.s.l. and sharing similar landslide movement characteristics with the Berceto (translational dormant landslide) and Carobbio (complex dormant landslide) landslides.

Through this process, we identified two cells analogous to the Carobbio landslide, encompassing the landslides of Marconi di Là in Ferriere (Piacenza) and Metti in Bore (Parma). These analogues are relatively distant from the Carobbio landslide, located 53 and 34 km away in the WNW direction. In contrast, we pinpointed one cell as an analogue for the Berceto landslide, containing the landslide of Bergotto - Corchia in Berceto (Parma). This third analogue is close to the Berceto landslide, approximately 3 km in the WSW direction (Fig. 7B).

4. Discussion

Landslides in the Northern Apennines are a prevalent feature of the landscape, making it one of the most landslide-prone areas in Italy (Bertolini, 2007). Several radiocarbon dates, collected over decades of research conducted on landslides (Tellini and Chelli, 2003; Bertolini et al., 2004, 2005; Soldati et al., 2006; Bertolini, 2007), have enabled us to analyse their distribution according to geographical features over time, primarily through the Holocene, and sparsely into periods preceding the LGM.

As we have found, out of the 95 dated samples from 43 landslides distributed in the Parma and Reggio-Emilia districts, only three samples from two landslides (the Berceto and Carobbio landslides) date back to before the LGM, and only five samples date to the Late Glacial period before the Holocene. The ancient organic material preserved within the landslides is of significant interest for paleoclimatic research, and landslides serve as important natural archives despite lacking continuous recording capabilities like those found in peat bogs and lacustrine sediments.

Organic remnants within a landslide body, often at varying depths and occasionally exposed at the surface, provide evidence of past landslide events. We categorised the landslides into two primary groups: recurrent (reactivating) and single-event landslides. One limitation of this classification is that some remnants may not have been recovered in the latter group, leading to the landslide being categorised as a single event rather than recurrent. Moreover, even within the recurrent landslides, it's possible that some remnants indicating a previous event may be lost. The absence of organic material within the investigated landslide body (and hence, dated events) can be attributed to several factors: (1) True lack of landslide activity. (2) Absent or sparse vegetation cover on the landslide surface (e.g., during extended cold periods lasting several years or after a landslide event that removes vegetation cover for decades). (3) Uneven distribution of remnants within the landslide body, making it possible to miss some remnants during sampling. (4)

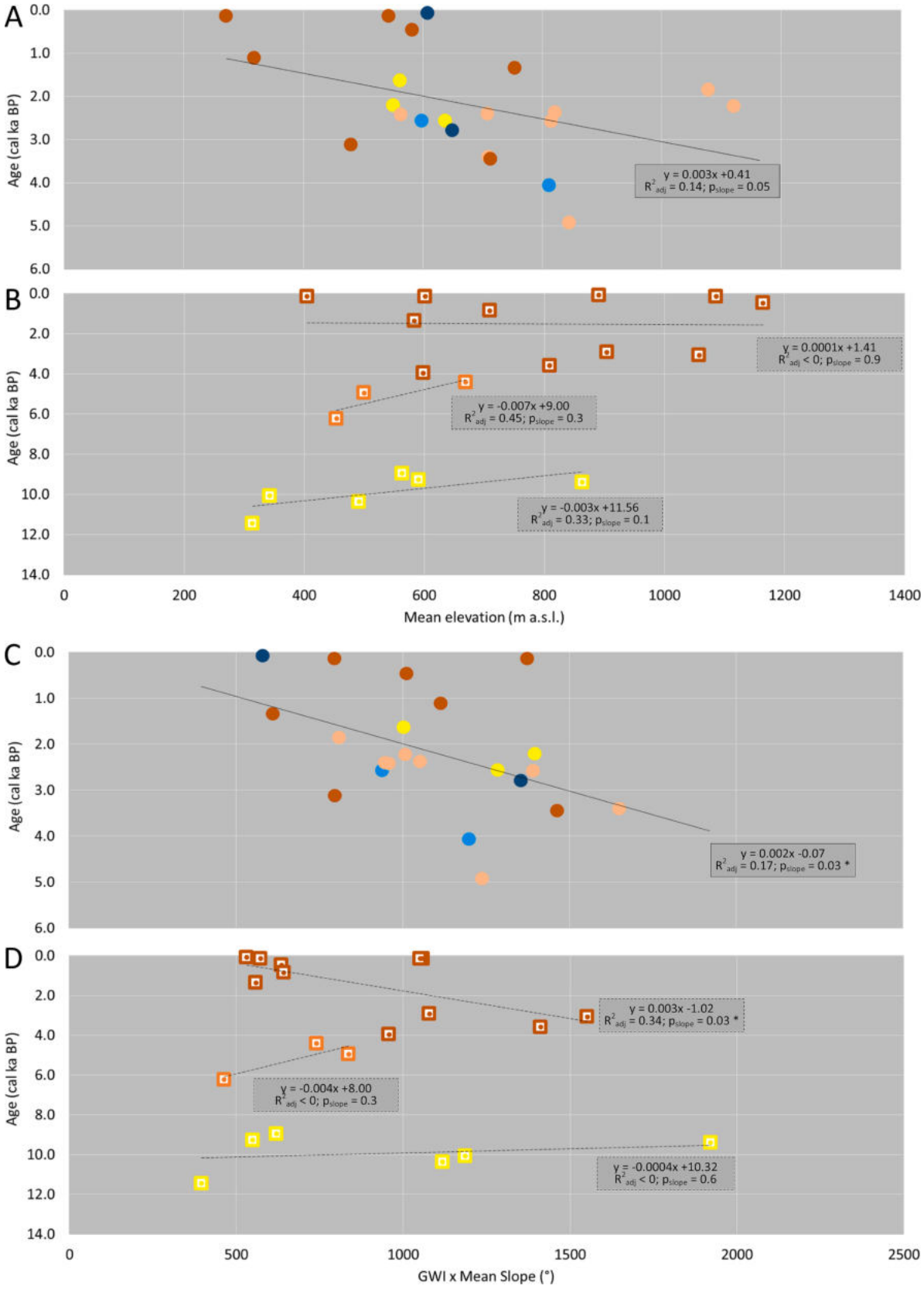

Fig. 4. Regression of the last (most recent) calibrated age obtained from a landslide, over the mean elevation of the grid cell containing the landslide (A, B), and over the variable GWI × Mean Slope (see Methods) reassuming lithotechnic and topographic characteristics of the grid cell containing the landslide (C, D). Symbols and colours, as in Fig. 3.

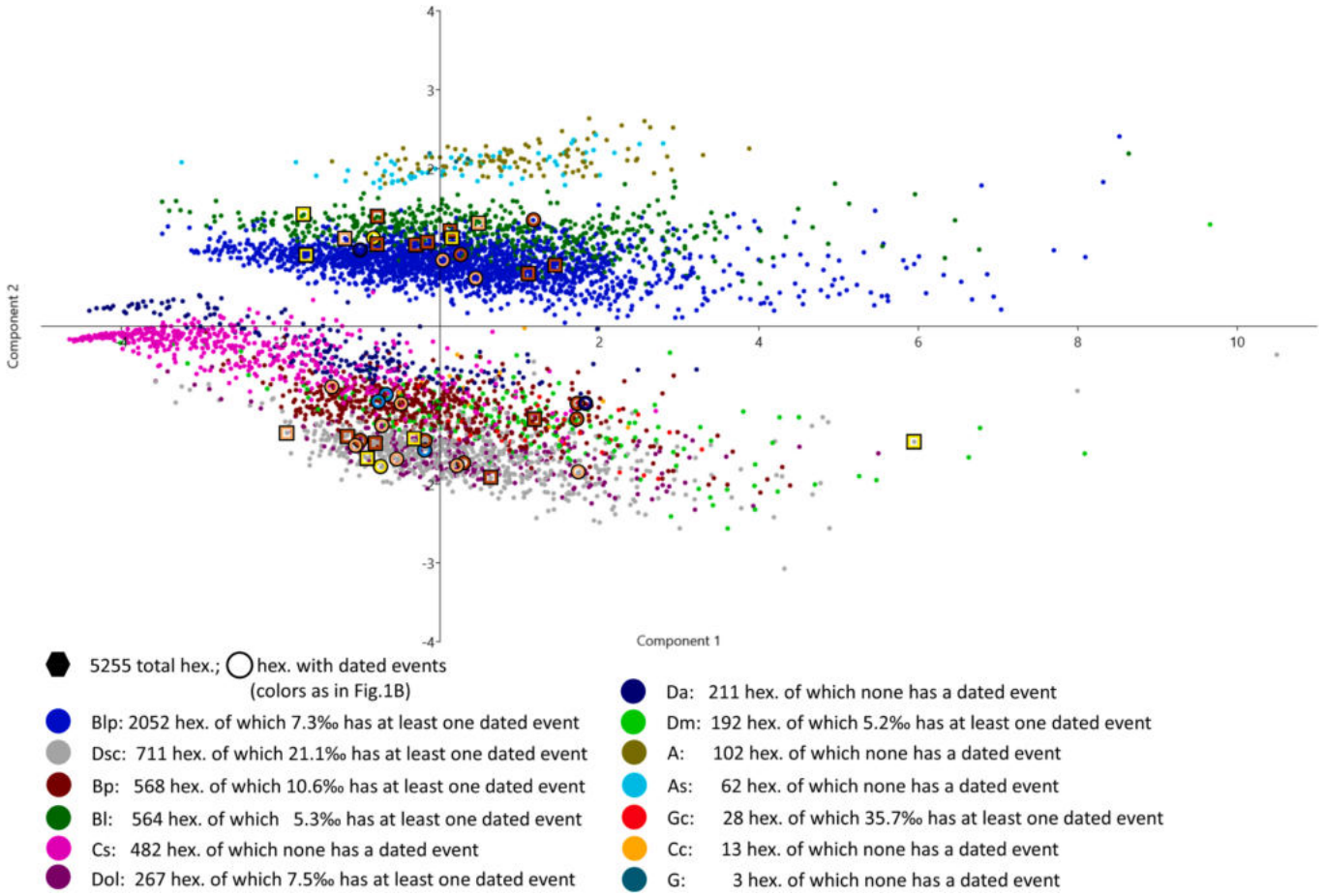

Fig. 5. Principal components analysis PCA of the 5255 grid cells in the whole study area (coloured points), distinguished by the main underlying lithology in each cell in terms of surface cover. The different lithotechnic characteristics of the rock masses are depicted in different colours: acronyms and details of the rock masses and associated rock types are explained in Table 2. Each grid cell comprising a dated landslide is surrounded either by a circle (recurrent landslides) or a square (single-event landslides), coloured according to the oldest calibrated date obtained (colours as in Fig. 1B). The legend at the bottom reports the main underlying lithologies from more to less frequent, and also the rate of cells presenting dated events in a landslide deposit concerning the total cells with the same rock masses underlying, in permil (‰).

Loss of remnants due to the degradation of organic matter, a process that could be slowed down by clayey lithologies in the deposits (such as Dsc, as in our research) or accelerated by sandstones and arenites (Cs) (e.g., Kibblewhite et al., 2015). Certain landslide types can also influence this process, such as rock falls or mudflows and debris flows.

Another factor contributing to the loss of organic remnants could be the reactivation of landslides during major events, which can displace remnants and disrupt the original stratigraphy. After these events, the previously buried organic remnants may frequently emerge at the surface in remarkably well-preserved conditions. However, they tend to degrade rapidly once exposed to meteorological factors and the oxidising environment.

Hence, the entire research is constrained by analysing only radiocarbon-dated landslide events, likely the most significant ones, and the limited availability of dates for just 43 landslides within the study region. Expanding the dataset with more dates from a broader range of landslides would undoubtedly enhance our ability to assess the robustness of the proposed model for the Holocene (Section 4.1) and the tentative reconstruction of related changes in atmospheric circulation (Section 4.2). Additionally, we introduce a method for exploring ancient remnants within the study region (Section 4.3).

4.1. Spatial patterns of landslide events: A model for the Holocene, with all dated events

Considering the scarcity of dates before the LGM and in the Late Glacial period, our analysis focused on events during the Holocene, encompassing 87 dated landslide events in the study region. The position of the LGMgt boundary used in this research represents the lower extent of the colder and wetter areas within the territory. This variable is closely associated with glacialism, and incorporates information about general climatic conditions, including also the atmospheric perturbations. In contrast, the elevation of the mountain divide may be more directly linked to temperature, with precipitation playing a secondary role along a general precipitation gradient. During the LGM, the study region exhibited relatively low equilibrium line altitudes (ELAs, ranging from 1200 to 1500 m a.s.l.), varying from the inner to the outer part of the mountain chain, which is indicative of high glacier accumulation rates (Giraudi, 2011). These elevated accumulation rates resulted from the intense precipitation associated with southerly storm tracks, as Baroni et al. (2018) discussed.

We generally observed stronger relationships with climate-related variables in recurrent landslides (Fig. 3A, 3C) than in single-event landslides (Fig. 3B, 3D). When considering only the most recent events in recurrent landslides and those of the single-event landslides, we noticed that all the events occurred at different periods concerning their proximity to either the position of the LGMgt or the primary mountain

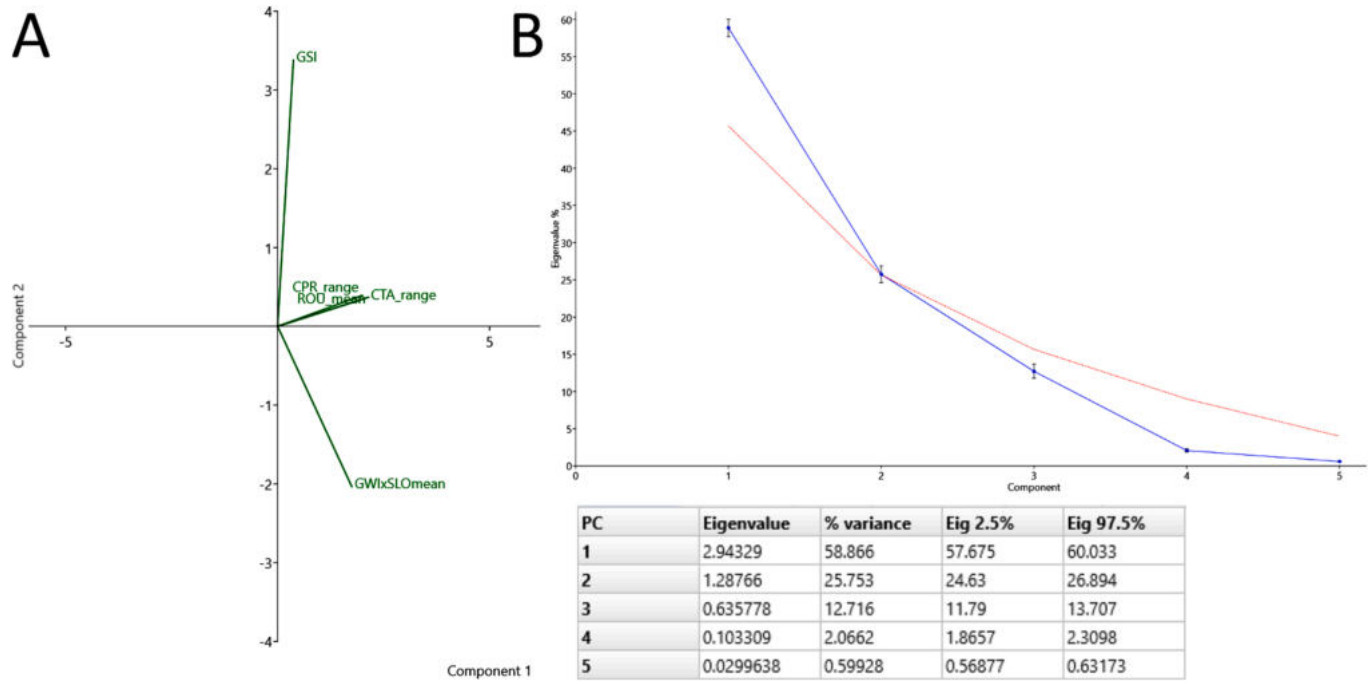

PC	Eigenvalue	% variance	Eig 2.5%	Eig 97.5%
1	2.94329	58.866	57.675	60.033
2	1.28766	25.753	24.63	26.894
3	0.635778	12.716	11.79	13.707
4	0.103309	2.0662	1.8657	2.3098
5	0.0299638	0.59928	0.56877	0.63173

Fig. 6. Graph associated with the PCA run of Fig. 5. (A) Projection of the original axes: component loadings highlighting the influence of the underlying variables on PC1 and PC2. Name of the explanatory variables: GSI geological strength index; GWI geological weakness index; SLO slope; CPR profile curvature; CTA tangential curvature; ROU roughness. (B) A Simple plot of eigenvalues indicates the significance of the first two components, explaining up to 84% of the total variance in the dataset (table at the bottom). The red line (broken stick) represents eigenvalues in a random model (Jackson. 1993). (For interpretation of the references to colour in this figure legend, the reader is referred to the web version of this article.)

divide in the south-west. However, distinct spatial patterns emerged between the two groups.

Regarding only the most recent events recorded, recurrent landslides, which remained active throughout the entire Holocene, exhibited a discernible spatial pattern in the upper Holocene. Earlier events were closer to the LGMgt positions, while later events occurred at greater distances from the LGMgt (Fig. 3A). This spatial pattern was also observed in the active single-event landslides during the upper Holocene (Fig. 3B). Notably, the significant difference between the two groups during the upper Holocene was that recurrent landslides showed a correlation with elevation, with landslides at higher elevations occurring first (and close to the LGMgt) and those at lower elevations occurring later (Fig. 4A). Conversely, the single-event landslides displayed no elevation-related pattern (Fig. 4B). However, both groups of dated events were initially concentrated on steep slopes and areas characterised by weak lithologies (Fig. 4C, 4D). Considering the lower Holocene, a reverse pattern emerged for single-event landslides. Earlier events were recorded further from the LGMgt position (and the primary mountain divide), while later events occurred closer to it (Fig. 3B, 3D). This was reflected in the lower altitudes of the earlier events and the higher altitudes of the later events (Fig. 4B). However, no significant correlation with slope or lithology was evident (Fig. 4D).

When examining the complete dataset of events for recurrent landslides throughout the Holocene, we can discern similar spatial patterns in both the lower and upper Holocene periods within these two groups of landslides (Fig. 8A). In the middle Holocene, single-event landslides were limited to only three occurrences, all located more than 10 km away from the position of the Last Glacial Maximum glacier terminus (LGMgt). In contrast, recurrent landslides (comprising 18 events) were predominantly concentrated in the upper region of the mountain chain, approximately 8.5 km from the LGMgt (only three events occurred at greater distances).

Considering the entire sequence of events spanning the Holocene, it becomes apparent that the initial events recorded by the landslides were situated in the lower portion of the mountain chain. Subsequently, they were primarily observed in the upper belt during the middle Holocene. Then, during the upper Holocene, events again shifted towards greater distances from the position of the LGMgt and the primary mountain divide.

The spatial patterns of events recorded in the lower Holocene, initially occurring in the lower section of the mountain chain and at greater distances from the LGMgt, may be attributed to a sequence of gravitational events and vegetation dynamics in response to climatic changes. Typically, following cooler periods, the recolonisation of slopes by vegetation commenced from lower elevations and glacial refugia, extending towards the colder regions at higher elevations. This process also influenced changes in the elevation of the treeline.

4.2. *Atmospheric changes derived from vegetation changes and landslide spatial patterns*

During the Late Glacial period and into the lower Holocene, the landscape was characterised by an open steppe woodland and shrubland featuring *Pinus* and *Artemisia*, although there were variations in vegetation and climatic conditions along both the west-east (W-E) axis and the north–south (N-S) slopes of the Northern Apennines. The south-facing slope of the mountain chain, being closer to the Mediterranean Sea and subjected to orographic precipitation, tended to be wetter than their north-facing counterparts, a pattern that persists in modern times.

During the Bølling-Allerød interstadial (Fig. 9A; Fig. 10A), the Alps experienced warm and dry conditions, leading to the expansion of *Picea* (Ravazzi, 2002). In contrast, the western sector of the Northern Apennines exhibited more humid conditions, as evidenced by the expansion of *Abies* and a corresponding decline in *Picea* (observed at the Lagdei and Berceto sites; Bertoldi, 1981, Lowe, 1992, Ravazzi, 2002, Bertoldi et al., 2004). Further to the east, *Pinus* and *Artemisia* continued to dominate the landscape, indicating drier conditions (Ravazzi et al., 2005).

During this period, we hypothesise that humid air masses moved westward and northward (similar to the LGM; as discussed by Baroni et al., 2018), impacting the mountain chain from the south but

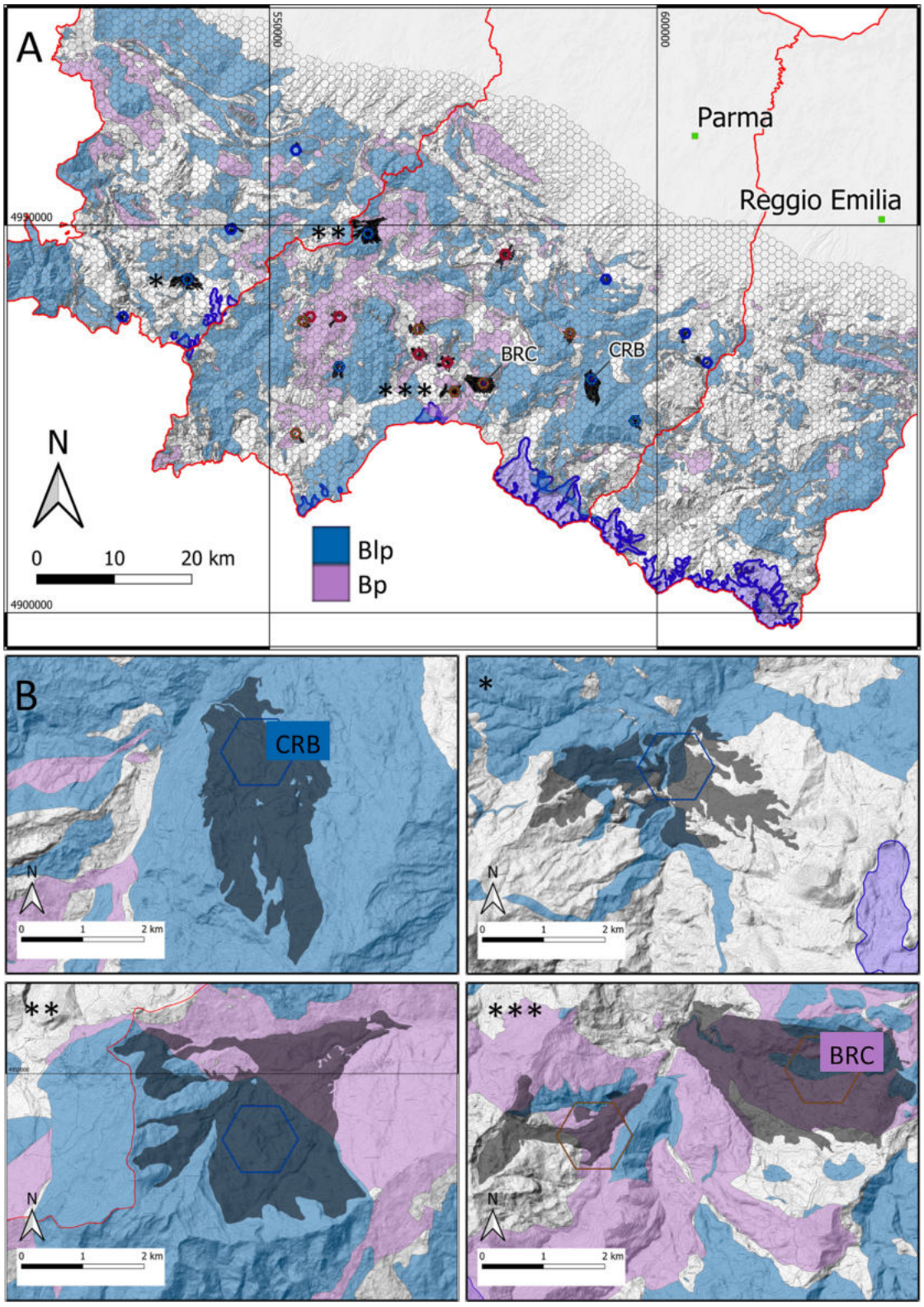

Fig. 7. Position of the 20 grid cells detected as analogue areas of the Berceto (BRC, red-coloured hollow hexagons) and the Carobbio (CRB, blue), landslides that dated back to periods before the LGM. The cells were detected based on the proximity in the PCA scatter plot, thus considering the underlying lithology and the topographic characteristics, such as roughness, curvature and slope. Areas of the comprised landslides are filled in black (A). A further selection has been performed by selecting the grid cells above 600 m a.s.l. as representing most likely similar environmental conditions of the Berceto and Carobbio landslides (cells at 649 and 608 m a.s.l., respectively): the hexagons of these grid cells are depicted with green dotted lines above the red or the blue colour. Finally, a further selection was applied, considering only those cells extensively presenting the same landslide movement as the one of Berceto (translational dormant landslide) and Carobbio (complex dormant landslide): these landslides are depicted in (B) at higher scales, with the corresponding asterisks: *, Marconi di Là in Ferriere (Piacenza); **, Metti in Bore (Parma); ***, Bergotto - Corchia in Berceto (Parma). The coordinates refer to the EPSG 25832, UTM Zone 32 N coordinate reference system. (For interpretation of the references to colour in this figure legend, the reader is referred to the web version of this article.)

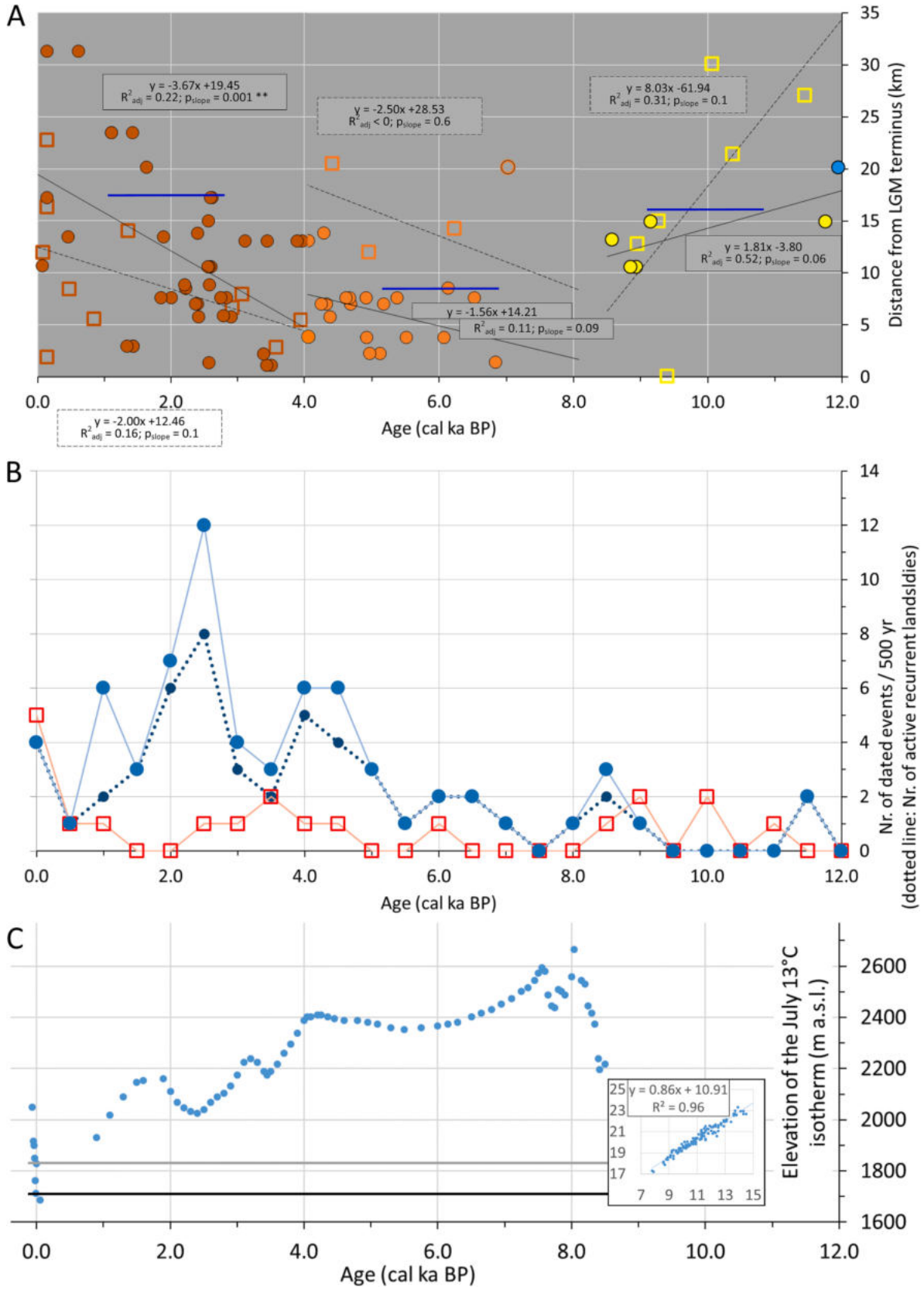

(caption on next page)

Fig. 8. All the 87 dated events of the Holocene plus one dating 11.9 cal ka BP (here included in the Holocene group) reported considering the distance from the LGMgt of the grid cells containing the recurrent (filled circles) and single-event (open squares) landslides as a function of age (A), respective equations and determination coefficients are also reported. In the group of the middle Holocene, the Metti landslide was omitted from the regression (hollow circle). The horizontal blue lines depict the 85th percentile of dated events for the group of recurrent landslides: this percentile was chosen considering the distribution of the events during the middle Holocene and then applied to the other two periods. The mid graph (B) depicts the number of dated events through the Holocene every 500 years, distinguishing between recurrent (light-blue line) and single-event (red line) landslides; the dotted blue line reports the number of active landslides within the recurrent ones. The bottom graph (C) depicts the elevation change of the July 13 °C isotherm through the Holocene, according to the temperature reconstruction of Badino et al. (2018), and modern values close the 0 cal years BP (i.e., 1950 CE) up to 2021 CE. The two horizontal lines represent the altitude of the main mountain divide in the south-west of the study area, considering only the portions above 1500 m a.s.l.: mean altitude 1710 m a.s.l. (black line), plus 1 standard deviation 1830 m a.s.l. (grey line); maximum altitude at Mt. Prado, 2054 m a.s.l. The bottom-right graph depicts the regression of modern July mean temperature of the five grid points in the Northern Apennines over the July mean temperature of the grid point in the Western Alps (1901–2021, CRU TS dataset, see Methods), the regression equation and the respective determination coefficient are also reported. (For interpretation of the references to colour in this figure legend, the reader is referred to the web version of this article.)

encountering resistance from dry air masses originating from the north. Additionally, it's worth noting that the Adriatic Sea during this time was situated farther from its modern position, approximately 90 m lower (Lambeck et al., 2004). This resulted in a drier environment and a climate with continental characteristics, likely influenced by air masses from the north.

During the Younger Dryas stadial (Fig. 9B; 10B), stronger air mass movements from the north may have induced colder conditions, leading to rapid changes in vegetation. In this period, *Pinus* and *Artemisia* expanded both on the south-facing slopes (Pian del Lago site, Guido et al., 2020) and on the north-facing slopes of the Northern Apennines (Lowe, 1992; Lowe and Watson, 1993; Bertoldi, 1981; Bertoldi et al., 2007; Vescovi et al., 2010).

During this period, the air masses from the south were somewhat weaker, resulting in drier conditions and a climate closer to the semiarid regime (Ravazzi, 2005) well established over the Po Plain region. Precipitation was at its lowest annual level since the LGM (Fig. 10F).

During the lower Holocene, we observed a spatial gradient of landslide events, initially recorded at greater distances from the Last Glacial Maximum glacier termina (LGMgt) and closer to it. This pattern may suggest a predominant influence of humid air masses originating from the Adriatic Sea, with a reduced contribution of intense precipitation from air masses from the south (Fig. 9C).

Throughout the lower Holocene, the increasing influence of humid air masses from the Adriatic Sea was associated with higher annual precipitation levels (Fig. 10C), a trend supported by the rapid expansion of *Abies* in locations such as Lake Greppo and eastern sites (Ravazzi et al., 2006). On the south-facing slope, this period corresponded to the expansion of *Abies*, along with declines in *Pinus* and, subsequently, *Artemisia*. Additionally, it marked the emergence of *Fagus*, accompanied by numerous other broadleaf species, including *Quercus*, *Corylus*, *Alnus*, *Fagus*, *Ostrya*, *Tilia*, *Ulmus*, and *Fraxinus*, which became dominant around 9970 cal. BP (Guido et al., 2020).

During the middle Holocene, a period characterised by very warm conditions, the Holocene Optimum (8000–6000 years BP) occurred. This period witnessed significant changes in the atmospheric circulation on a larger scale, as the intertropical convergence zone (ITCZ) shifted from approximately 20°N to 18°N. This shift likely contributed, not solely due to climatic factors, to the emergence of the Sahara Desert and the conclusion of the African Humid Period (8000–4500 years ago; Wright, 2017). The southward movement of the ITCZ led to a weakening of the Hadley cell, resulting in an increased influence of the humid air masses from the westerlies in the Mediterranean and our region (Magny et al., 2012).

Our findings indicate that landslide activity during this period was predominantly confined to a narrow zone located less than 8.5 km from the Last Glacial Maximum glacier termina (LGMgt) (Fig. 9D). This suggests that air masses from the south likely did not traverse the entire mountain range, and the eastern air masses did not significantly contribute to instability. The most intense precipitation events were likely concentrated in the higher elevations near the main mountain divide. The initial peak of landslide events in our study region occurred during the period 4.5–4.0 ka BP, during which recurrent landslides increased from an approximate rate of one event every 500 years (with a maximum of three events from two landslides) to a rate of up to six events every 500 years (involving four and then five landslides). These findings point to intense rainfall events (Fig. 8B). Notably, this period encompasses the 4.2 ka BP event, one of the Holocene's abrupt climatic changes. This event endured for approximately four centuries (Perry and Hsu, 2000; Mayewski et al., 2004; Magny et al., 2009) and marked the transition from the warm and wet conditions of the middle Holocene (i.e., from ~8.3 to ~4.2 ka BP) to the cooler and drier (with respect to the 4.2 ka BP event) conditions of the upper Holocene. After the 4.2–3.8 ka BP event, cooler summer conditions were also observed in the western European Alps (Badino et al., 2018), leading to glacier advances (Bortenschlager, 1982). These conditions likely extended to our study region, given the strong correlations found in modern temperature datasets (Fig. 8C).

During the middle Holocene (Fig. 9D), *Fagus* trees underwent significant expansion in the region, often replacing pure *Abies* forests at higher altitudes. This expansion began earlier, around 5800–5000 years BP, in the eastern part of the Northern Apennines, where the taller peaks allowed for greater precipitation and humidity, thereby favouring the proliferation of Alnus as well. This expansion then proceeded westward towards locations like Lake Moo and Lake Casanova, occurring between 4600 and 3000 years BP (Watson, 1996).

In the upper Holocene, *Fagus* successfully established itself at the treeline, and to this day, the current treeline in the study region predominantly consists of *Fagus*. Its elevation correlates with the July 13 °C isotherm (Pezzi et al., 2008; Rita et al., 2023). It's worth noting that the elevation of this isotherm has varied over time, with it being situated at approximately 2400 m a.s.l. during the middle Holocene, surpassing even the highest peaks in the region (Fig. 8C, estimated based on the reconstruction by Badino et al., 2018). Throughout the upper Holocene, there was a gradual trend of summer cooling that affected both the Alps and the study region, although there were occasional periods of temperature increase leading up to the recent warming (Fig. 8C).

In the upper Holocene, our results indicate a gradual transition of landslide events from the dividing area in the south toward the base of the mountain chain (Fig. 9E). This suggests a stronger circulation of humid air masses originating from the south, including storms from the westerlies and the Adriatic Sea. The air mass circulation patterns over the study region are predominantly influenced by the North Atlantic Oscillation (NAO), a dipole oscillation in sea-level pressure between the Icelandic low and the Azores high (subtropical) as described by Lamb and Pepler (1987). The NAO significantly shapes both winter and summer weather conditions across Northern and Southern Europe, as highlighted by Folland et al. (2009).

The study area's eastern (E) and western (W) parts experience the influx of humid air masses originating from the Adriatic and Mediterranean Seas, respectively. The south-facing slope of the mountain chain receives higher levels of precipitation. During a positive NAO phase, Southern Europe exhibits dry and cooler conditions, whereas during a negative NAO phase, the weather becomes characterised by wetter and

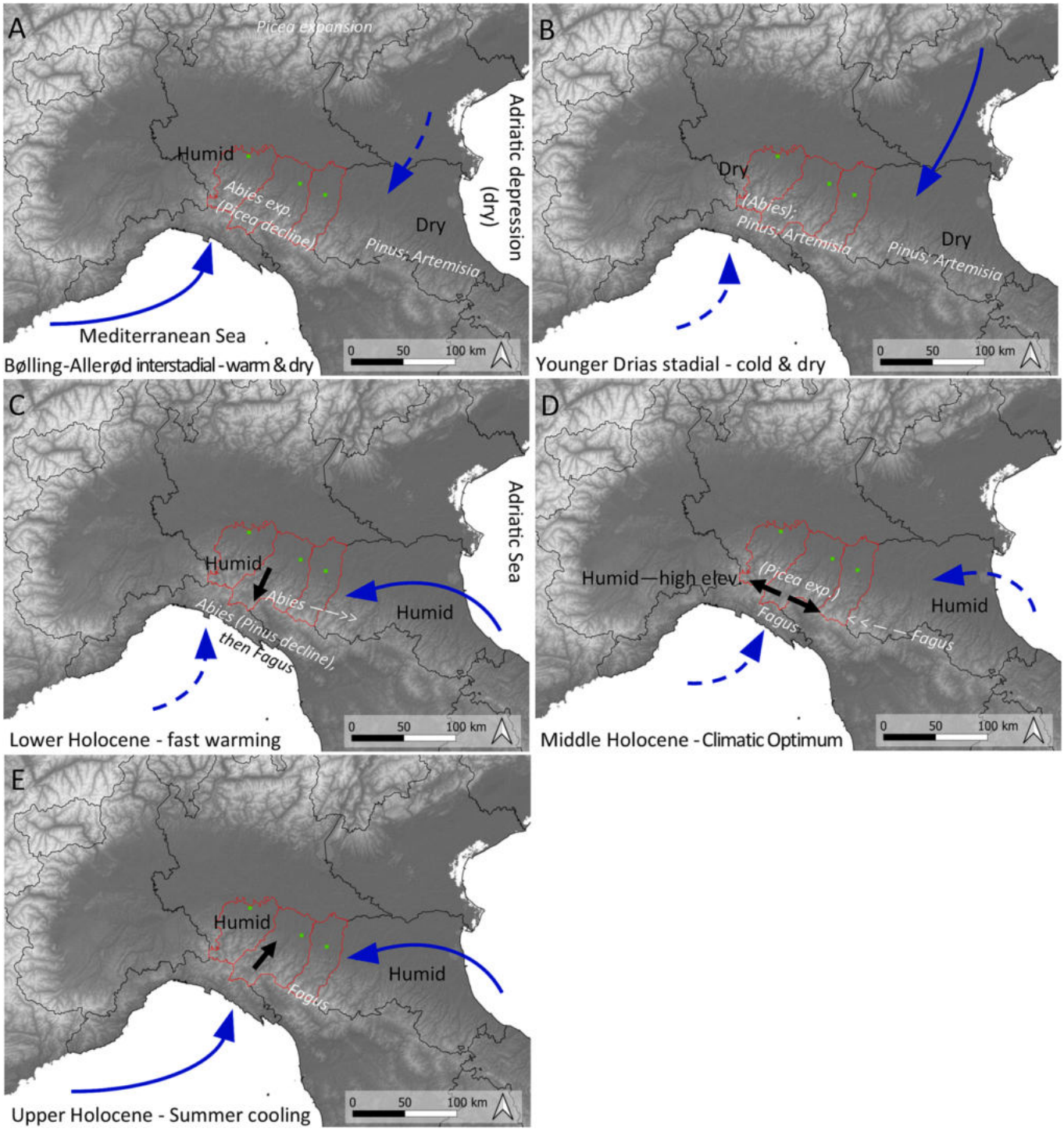

Fig. 9. Tentative reconstruction of main directions of air masses and storm tracks for humid air masses over the study region in the Late Glacial (A, B) and the Holocene (C, D, E), derived from vegetation changes (from literature data) and from the landslide spatial patterns during the Holocene (from this work). Directions of landslide spatial patterns are depicted with black arrows for the whole Holocene. Blue arrows depict the dominant direction of air masses (strong conditions, full and long lines; weak conditions, short and dashed lines). (For interpretation of the references to colour in this figure legend, the reader is referred to the web version of this article.)

warmer conditions.

During the upper Holocene, we observed the most intense landslide activity occurring between 3.0 ka BP and 2.0 ka BP. This period exhibited the highest concentration of recorded events in the dataset, with up to 12 events per 500 years originating from eight active landslides, followed by seven events per 500 years from six active landslides. This trend, however, is not observed in the group of single-event landslides, whose maximum value occurs in the last 500 years of the dataset, with five events recorded. These single-event landslides were located at great distances from the LGMgt, on low dip slopes, and in areas with weak lithologies.

This peak in events corresponds to a period of further summer cooling, as illustrated in Fig. 8C. It can also be attributed to more intense precipitation affecting the area, starting initially at its southern limit and

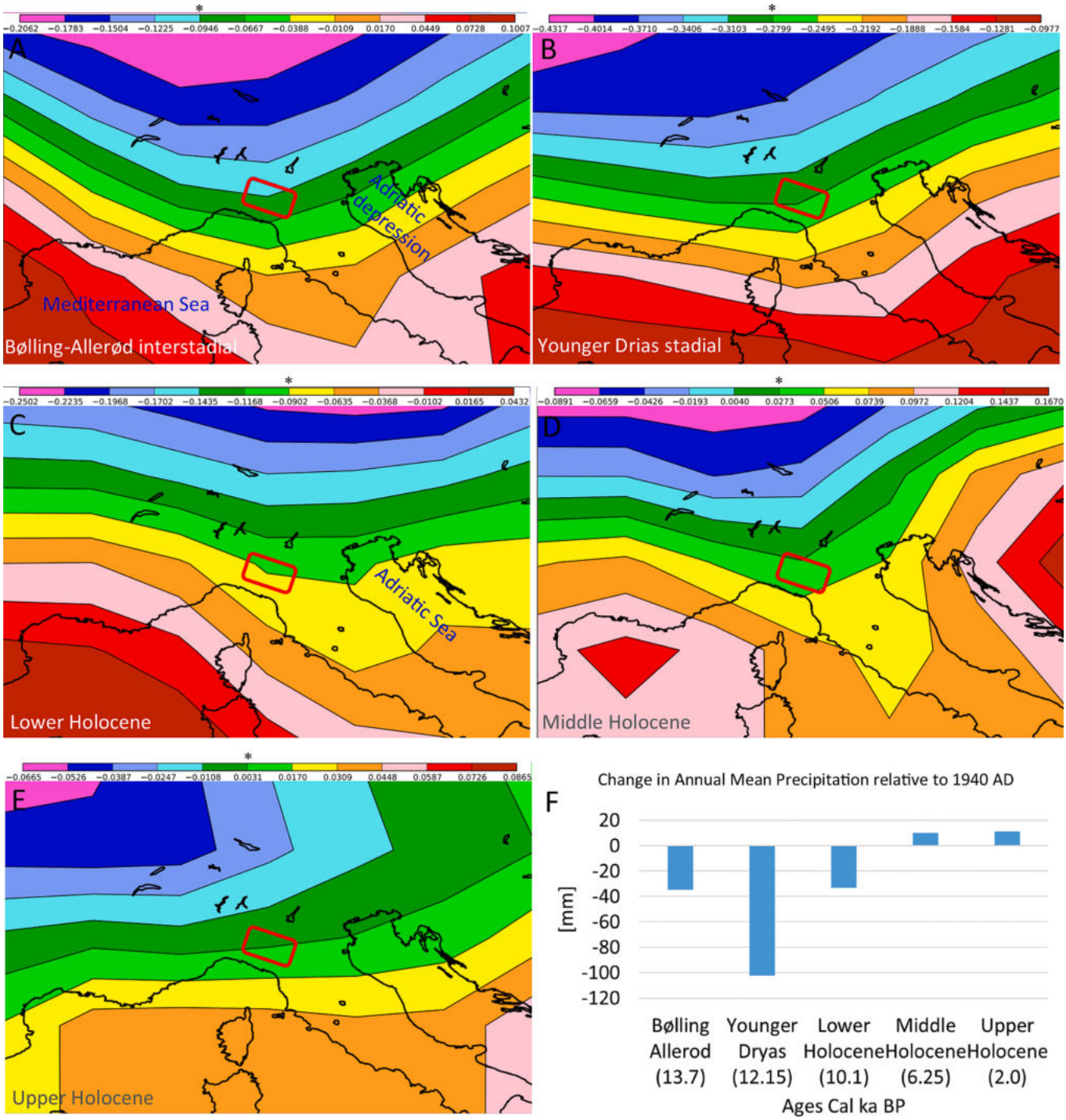

Fig. 10. Change in annual mean precipitation with respect to 1940 CE (most recent year available) in the central periods of Bølling-Allerod (13.7 cal ka BP), Younger Dryas (12.15 cal ka BP), Lower to Upper Holocene (10.1, 6.25, and 2.0 cal ka BP), expressed as mm/day, over the region around the study area (red rectangle) based on the PaleoView model (Fordham et al., 2017). Climate data are averaged over 100 years, and the daily changes are reported in the legend at the top of each frame (10A to 10E). Note that each legend has different intervals. The change of annual mean precipitation expressed in mm/year during the same periods is also depicted (10F): values derived from mm/day (see asterisks above the legends). (For interpretation of the references to colour in this figure legend, the reader is referred to the web version of this article.)

progressing northward. Interestingly, a similar concentration of dated landslide events is also recorded in the Polish flysch Carpathians at 2.3–1.9 ka BP (Margielewski, 2002). This observation underscores a common climatic influence on landslide events across central and Southern Europe.

4.3. Territorial features promoting the conservation of datable materials

The PCA analysis of the sampled landslides reveals a notable pattern: certain areas, characterised by intensely tectonised clay shales (Dsc) as their underlying lithology, exhibit a high frequency of dated events. Conversely, areas with lightly cemented sandstones and arenites exhibits no dates of landslide events. These contrasting conditions suggest

that lithology plays a crucial role in this phenomenon, as it directly influences the presence of underground water and air within the deposits. Specifically, soils rich in clay and fine texture are identified as the most effective types for preserving organic remnants. This is due to their ability to facilitate absorption and occlusion in the soil matrix (Kibblewhite et al., 2015) and create anaerobic conditions (Bjordal et al., 1999; Douterelo et al., 2010).

The ancient organic matter contained within the landslides holds significant paleoclimatic value. With this perspective in mind, we have devised a method to identify regions that closely resemble the conditions present in two active landslides even before the LGM, namely, the Berceto and Carobbio landslides. Utilising PCA and considering the varying underlying lithologies (Bp for Berceto and Blp for Carobbio), we have successfully pinpointed areas that exhibit similarities also in topography and elevation. These identified landslides can, therefore, serve as promising sites for future investigations aimed at uncovering ancient organic remnants.

In addition to targeting the retrieval of the oldest organic remnants, our method, built upon our discoveries, can be systematically employed to sample landslides. This includes the incorporation of underrepresented lithologies and landslide types, facilitating a precise reconstruction of the spatial dynamics that have unfolded over millennia. Furthermore, our spatial dynamics model, which relies on distances from cooler regions within the territory, holds promise for application and testing in other mountain ranges where numerous landslide event dates are accessible.

5. Conclusions

Our analysis has highlighted a noteworthy aspect beyond the well-established correlation between climate and landslide activity, typically observed from a temporal perspective. In the case of the north-facing slope of the Northern Apennines, landslide events during the Holocene have demonstrated distinct spatial patterns. Specifically, in the Early Holocene, events occurred first in the lower reaches of the mountain chain, far from the Last Glacial Maximum glacier termina (LGMgt). In the Middle Holocene, most landslide events occurred within approximately 8.5 km from the LGMgt. They were located in the inner sections of the mountain chain, with the highest concentration clustering during the period encompassing the 4.2 ka BP event. In the upper Holocene, landslide events were primarily situated close to the LGMgt and then extended further away, with the highest concentration occurring during the initial phases, from 3.0 ka BP to 2.0 ka BP. These patterns in landslide events and shifts in vegetation composition mirror alterations in the circulation patterns of air masses across the region.

Furthermore, our analysis enabled the identification of landslides exhibiting anomalous behaviour, including the absence of significant events recorded (by remnants) for over 8000 years, as seen in the Beduzzo landslide, possibly due to the non-preservation or non-retrieval of organic material; unanticipated activity occurring at distances exceeding 20 km from the LGMgt, while most landslide events are typically confined within 8.5–10 km from the LGMgt, as observed in the Metti landslide; and landslides occurring outside the primary cluster in the PCA space, primarily due to topographical factors, exemplified by the Succiso landslide.

Our approach has identified disparities in the representation of landslide events across territories characterised by different underlying lithologies. Notably, areas with intensely tectonised clay shales exhibit a significantly higher frequency of dated events, with a rate of cells containing a dated landslide (21.1 ‰) roughly triple that of the most widespread lithology in the region (flysch formations).

Lastly, our analysis has allowed us to identify landslides analogous to those of Berceto and Carobbio, which were already active before the LGM. This result provides a valuable research direction for retrieving ancient organic material. Such material not only aids in dating landslide events but also offers invaluable climatic information.

Declaration of Competing Interest

The authors declare that they have no known competing financial interests or personal relationships that could have appeared to influence the work reported in this paper.

Data availability

Data will be made available on request.

Acknowledgements and Funding

This research is dedicated to Prof. Claudio Tellini, who recently passed away and whose research was mainly focused on geomorphology and landslides of the Northern Apennines in the Parma district, extensively collecting wood remnants and performing ^{14}C dating of landslide events.

This work has benefited from the equipment and framework of the COMP-HUB and COMP-R Initiatives, funded by the 'Departments of Excellence' program of the Italian Ministry for University and Research (MIUR, 2018-2022 and MUR, 2023-2027). The work was supported by the research fund CHELLI_A_FIL University of Parma (Head: A. Chelli) and the research fund LEONELLI_G_FIL University of Parma (Head: G. Leonelli). The Authors acknowledge the Editor and the two anonymous reviewers for the deep revision of the manuscript and the useful suggestions that greatly improved the text.

References

Badino, F., Ravazzi, C., Valle, F., Pini, R., Aceti, A., Brunetti, M., Champvillair, E., Maggi, V., Maspero, F., Perego, R., Orombelli, G., 2018. 8800 years of high-altitude vegetation and climate history at the Rutor Glacier forefield, Italian Alps. Evidence of middle Holocene timberline rise and glacier contraction. Quat. Sci. Rev. 185, 41–68. https://doi.org/10.1016/j.quascirev.2018.01.022.

Baroni, C., Guidobaldi, G., Salvatore, M.C., Christl, M., Ivy-Ochs, S., 2018. Last glacial maximum glaciers in the Northern Apennines reflect primarily the influence of southerly storm-tracks in the western Mediterranean. Quat. Sci. Rev. 197, 352–367. https://doi.org/10.1016/j.quascirev.2018.07.003.

Bertoldi, R., 1981. Le vicende vegetazionali e climatiche nella sequenza paleobotanica würmiana e post-würmiana di Lagdei (Appennino Settentrionale). Ateneo Parmense, Acta Naturalia 16, 147–175.

Bertoldi, R., Chelli, A., Roma, R., Tellini, C., Vescovi, P., 2004. First remarks on late Pleistocene lacustrine deposit in the Berceto area (Northern Apennines, Italy). Il Quaternario 17 (2/1), 133–143.

Bertoldi, R., Chelli, A., Roma, R., Tellini, C., 2007. New data from Northern Apennines (Italy) pollen sequences spanning the last 30,000 yrs. Il Quaternario - Italian Journal of Quaternary Sciences 20 (1), 3–20.

Bertolini, G., Casagli, N., Ermini, L., Malaguti, C., 2004. Radiocarbon data on Lateglacial and Holocene landslides in the Northern Apennines. Nat. Hazards 31, 645–662. https://doi.org/10.1023/B:NHAZ.0000024896.34933.63.

Bertolini, G., Guida, M., Pizziolo, M., 2005. Landslides in Emilia-Romagna region (Italy): strategies for hazard assessment and risk management. Landslides 2, 302–312. https://doi.org/10.1007/s10346-005-0020-1.

Bertolini, G., Corsini, A., Tellini, C., 2017. Fingerprints of Large-Scale Landslides in the Landscape of the Emilia Apennines. In: Soldati, M., Marchetti, M. (Eds.), Landscapes and Landforms of Italy, World Geomorphological Landscapes. Springer International Publishing, Cham, pp. 215–224. https://doi.org/10.1007/978-3-319-26194-2_18.

Bertolini, G., 2007. Radiocarbon dating on landslides in the Northern Apennines (Italy). In: McInnes, R., Jakeways, J., Fairbank, H. (Eds.), Landslides and Climate Changes: Challenges and Solutions, Proceedings of the International Conference on Landslides and Climate Change. Taylor & Francis, Ventnor, Isle of Wight, 21–24 May 2007, UK: pp. 73-80; https://doi.org/10.1201/NOE0415443180.

Bettelli, G., Bollettinari, G., Carton, A., Castaldini, D., Panizza, M., Piacente, S., Bernini, M., Clerici, A., Tellini, C., Vittorini, S., Canuti, P., Moisello, U., Tenti, G., Dramis, F., Gentili, B., Pambianchi, G., Bidini, D., Lulli, L., Rodolfi, G., Busoni, E., Ferrari, G., Cremaschi, M., Marchesini, A., Accorsi, C.A., Bandini Mazzanti, M., Francavilla, F., Marchetti, G., Vercesi, P.L., Di Gregorio, F., Marini, A., 1982. Geomorfologia del territorio di Febbio tra il M. Cusna e il F. Secchia (Appennino Emiliano). Geogr. Fis. Din. Quat. 5, 285–360.

Bettelli, G., De Nardo, M.T., 2001. Geological outlines of the Emilia Apennines (northern Italy) and introduction to the formations surrounding the landslides which resumed activity in the 1994–1999 period. In: Bertolini, G., Pellegrini, M., Tosatti, G. (Eds.), Le Frane della Regione Emilia Romagna, oggetto di interventi di Protezione Civile nel Periodo 1994–1999, Quaderni di Geologia Applicata, 8(1). Pitagora Editore, Bologna, pp. 1–26.

Bjordal, C., Nilsson, T., Daniel, G., 1999. Microbial decay of waterlogged archaeological wood found in Sweden applicable to archaeology and conservation. Int. Biodeterior. Biodegrad. 43, 63–73.
Borgatti, L., Soldati, M., 2002. The influence of Holocene climatic changes on landslide occurrence in Europe. In: Rybar, J., Stemberk, J., Wagner, P. (Eds.), Landslides. Balkema, Rotterdam, pp. 111–116.
Borgatti, L., Soldati, M., 2010. Landslides as a geomorphological proxy for climate change: A record from the Dolomites (northern Italy). Geomorphology 120, 56–64. https://doi.org/10.1016/j.geomorph.2009.09.015.
Bortenschlager, S., 1982. Chronostratigraphic subdivisions of the Holocene in the Alps. Striae 16, 75–79.
Carlini, M., Chelli, A., Vescovi, P., Artoni, A., Clemenzi, L., Tellini, C., Torelli, L., 2016. Tectonic control on the development and distribution of large landslides in the Northern Apennines (Italy). Geomorphology 253, 425–437. https://doi.org/10.1016/j.geomorph.2015.10.028.
Carlini, M., Chelli, A., Francese, R., Giacomelli, S., Giorgi, M., Quagliarini, A., Carpena, A., Tellini, C., 2018. Landslides types controlled by tectonics-induced evolution of valley slopes (Northern Apennines, Italy). Landslides 15, 283–296. https://doi.org/10.1007/s10346-017-0871-2.
Chelli, A., Tellini, C., 2002. Geomorphological features ofthe Bratica Valley (Northern Apennines, Italy). Geogr. Fis. Dinam. Quat. 25 (1), 45–60.
Compostella, C., Mariani, G.S., Trombino, L., 2014. Holocene environmental history at the treeline in the Northern Apennines, Italy: A micromorphological approach. The Holocene 24, 393–404. https://doi.org/10.1177/0959683613518588.
Corominas, J., Moya, J., 2008. A review of assessing landslide frequency for hazard zoning purposes. Engineering Geology 102, 193–213.
Cremaschi, M., 1990. The loess in Northern and Central Italy. A loess basin between the Alps and the Mediterranean Region. Quaderni di Geodinamica Alpina e Quaternaria 1, Milano.
Dapples, F., Oswald, D., Raetzo, H., 2002. Holocene landslide activity in the Western Swiss Alps – a consequence of vegetation changes and climate oscillations. In: Rybar, J., Stemberk, J., Wagner, P. (Eds.), Landslides. Balkema, Rotterdam, pp. 349–354.
Douterelo, I., Goulder, R., Lillie, M., 2010. Soil microbial community response to land-management and depth, related to the degradation of organic matter in English wetlands: implications for the in situ preservation of archaeological remains. Appl. Soil Ecol. 44 (3), 219–227.
Elenga, H., Peyron, O., Bonnefille, R., Prentice, I.C., Jolly, D., Cheddadi, R., Guiot, J., Andrieu, V., Bottema, S., Buchet, G., de Beaulieu, J.-L., Hamilton, A.C., Maley, J., Marchant, R., Perez-Obiol, R., Reille, M., Riollet, G., Scott, L., Straka, H., Taylor, D., Van Campo, E., Vincens, A., Laarif, F., Jonson, H., 2000. Pollen-based biome reconstructions for southern Europe and Africa 18,000 yr BP. J. Biogeogr. 27, 621–634.
Federici, P.R., Tellini, C., 1983. La geomorfologia dell'alta Val Parma (Appennino settentrionale). Riv. Geogr. It. 90, 393–428.
Folland, C.K., Knight, J., Linderholm, H.W., Fereday, D., Ineson, S., Hurrell, J.W., 2009. The Summer North Atlantic Oscillation: past, present and future. J. Clim 22, 1082–1103.
Fordham, D.A., Saltré, F., Haythorne, S., Wigley, T.M.L., Otto-Bliesener, B.L., Chan, K.C., Brook, B.W., 2017. PaleoView: a tool for generating continuous climate projections spanning the last 21000 years at regional and global scales. Ecography 40, 1348–1358.
Gariano, S.L., Guzzetti, F., 2016. Landslides in a changing climate. Earth Sci. Rev. 162 (2016), 227–252. https://doi.org/10.1016/j.earscirev.2016.08.011.
Giraudi, C., 2004. The Apennine glaciations in Italy. In: Ehlers, J., Gibbard, P.L. (Eds.), Quaternary Glaciations - Extent and Chronology, Part I: Europe. Developments in Quaternary Science 2. Elsevier, Amsterdam, pp. 215–223.
Giraudi, C., Frezzotti, M., 1997. Late Pleistocene glacial events in the Central Apennine. Italy. Quatern. Res. 48, 280–290.
Giraudi, C., 2011. Middle Pleistocene to Holocene glaciations in the Italian Apennines. In: Ehlers, J., Gibbard, P.L., Hughes, P.D. (Eds.), Quaternary Glaciations - Extent and Chronology: a Closer Look. Developments in Quaternary Science (15). Elsevier, Amsterdam, pp. 211–219.
Guido, M.A., Molinari, C., Moneta, V., Branch, N., Black, S., Simmonds, M., Stastney, P., Montanari, C., 2020. Climate and vegetation dynamics of the Northern Apennines (Italy) during the Late Pleistocene and Holocene. Quat. Sci. Rev. 231, 106206 https://doi.org/10.1016/j.quascirev.2020.106206.
Hammer, Ø., Harper, D.A.T., Ryan, P.D., 2001. PAST: Paleontological Statistics Software Package for Education and Data Analysis. Palaeontologia Electronica 4(1), 9 pp., ver. 4.08.
Harris, I., Osborn, T.J., Jones, P., Lister, D.H., 2020. Version 4 of the CRU TS monthly high-resolution gridded multivariate climate dataset. Sci Data 7, 109. https://doi.org/10.1038/s41597-020-0453-3.
Hoek, E., Brown, E.T., 1997. Practical estimates of rock mass strength. Int. J. Rock Mech. Min. Sci. 34 (8), 1165–1186.
Hughes, P.D., Woodward, J.C., 2008. Timing of glaciation in the Mediterranean mountains during the last cold stage. J. Quat. Sci. 23, 575–588.
ISPRA, 2021. Inventory of landslides in Italy IFFI project. Report APAT 78/2007, ISBN: 978-88-448-0310-0 https://www.isprambiente.gov.it/en/projects/soil-and-territory/iffi-project.
Jackson, D.A., 1993. Stopping rules in principal components analysis: a comparison of heuristical and statistical approaches. Ecology 74, 2204–2214.
Kibblewhite, M., Tóth, G., Hermann, T., 2015. Predicting the preservation of cultural artefacts and buried materials in soil. Sci. Total Environ. 529, 249–263.
Korup, O., Densmore, A.L., Schlunegger, F., 2010. The role of landslides in mountain range evolution. Geomorphology 120, 77–90. https://doi.org/10.1016/j.geomorph.2009.09.017.
L'Abée-Lund, J.H., Haugland, S., Melvold, K., Saltveit, S.J., Eie, J.A., Hvidsten, N.A., Pettersen, V., Faugli, P.E., Jensen, A.J., Pettersson, L.-E., 2009. In: Tockner, K., Uehlinger, U., Robinson, C.T. (Eds.), Rivers of the Boreal Uplands. Rivers of Europe. Academic Press, pp. 577–606. https://doi.org/10.1016/B978-0-12-369449-2.00015-1.
L'Abée-Lund, J.H., Aamodt, K.O., Brittain, J.E., Eie, J.A., Faugli, P.E., Haugland, S., Hvidsten, N.A., Jensen, A.J., Melvold, K., Pettersen, V., Saltveit, S.J., 2021. In: Tockner, K., Zarfl, C., Robinson Rivers of Europe, 2nd edition. Elsevier, Amsterdam, The Netherlands, ISBN: 9780081026120, pp. 777–811., C.T. (Eds.).
Lamb, P.J., Pepler, R.A., 1987. North Atlantic Oscillation: concept and application. Bulletin of American Meteorological Society 68, 1217–2122.
Lambeck, K., Antonioli, F., Purcell, A., Silenzi, S., 2004. Sea-level change along the Italian coast for the past 10,000 yr. Quat. Sci. Rev. 23, 1567–1598.
Lang, A., Moya, J., Corominas, J., Schrott, L., Dikau, R., 1999. Classic and new dating methods for assessing the temporal occurrence of mass movements. Geomorphology 30 (1–2), 33–52. https://doi.org/10.1016/S0169-555X(99)00043-4.
Larsen, I.J., Montgomery, D.R., 2012. Landslide erosion coupled to tectonics and river incision. Nat. Geosci. 5, 467–473.
Lowe, J.J., 1992. Lateglacial and early Holocene lake sediments from the Northern Apennines, Italy – pollen stratigraphy and radiocarbon dating. Boreas 21, 193–208.
Lowe, J., Watson, C.S., 1993. Lateglacial and Holocene pollen stratigraphy of the northern Apennines. Italy. Quat. Sci. Rev. 12, 727–738.
Magny, M., Vanniere, B., Zanchetta, G., Fouache, E., Touchais, G., Petrika, L., Coussot, C., Walter-Simonnet, A.-V., Arnaud, F., 2009. Possible complexity of the climatic event around 4300–3800 cal. BP in the central and western Mediterranean. The Holocene 19, 823–833.
Mandrone, G., 2004. Assessing the geomechanical features of some of the most common heterogeneous rock units in the Northern Apennines. Quaderni di Geologia Applicata 11 (2), 5–18.
Margielewski, W., 2002. Landslides. Balkema, Rotterdam, pp. 399–404.
Marinos, P., Hoek, E., 2000. GSI-A geologically friendly tool for rock mass strength estimation. Proceedings of the International Conference on Geotechnical and Geological Engineering (GeoEng2000), Melbourne, 1422-1442.
Marinos, V., Marinos, P., Hoek, E., 2005. The geological strength index: applications and limitations. Bull. Eng. Geol. Environ. 64, 55–65. https://doi.org/10.1007/s10064-004-0270-5.
Mayewski, P.A., Rohling, E.E., Stager, J.C., Karlén, W., Maasch, K.A., Meeker, L.D., Meyerson, E.A., Gasse, F., van Kreveld, S., Holmgren, K., Lee-Thorp, J., Rosqvist, G., Rack, F., Staubwasser, M., Schneider, R.R., Steig, E.J., 2004. Holocene climate variability. Quat. Res. 62, 243–255.
Molli, G., 2008. Northern Apennine-Corsica orogenic system: An updated overview. Geochem. Soc. Spec. Publ. 298, 413–442. https://doi.org/10.1144/SP298.19.
Myhre, G., Alterskjær, K., Stjern, C.W., Hodnebrog, Ø., Marelle, L., Samset, B.H., Sillmann, J., Schaller, N., Fischer, E., Schulz, M., Stohl, A., 2019. Frequency of extreme precipitation increases extensively with event rareness under global warming. Sci. Rep. 9, 16063. https://doi.org/10.1038/s41598-019-52277-4.
Pánek, T., 2019. Landslides and Quaternary climate changes—The state of the art. Earth-Science Reviews 196, 102871. https://doi.org/10.1016/j.earscirev.2019.05.015.
Perry, C.A., Hsu, K.J., 2000. Geophysical, archaeological, and historical evidence support a solar-output model for climate change. PNAS 97 (23), 12433–12438.
Pezzi, G., Ferrari, C., Corazza, M., 2008. The Altitudinal Limit of Beech Woods in the Northern Apennines (Italy). Its Spatial Pattern and Some Thermal Inferences. Folia Geobot 43, 447–459. https://doi.org/10.1007/s12224-008-9025-6.
Ponel, P., Lowe, J.J., 1992. Coleopteran, pollen and radiocarbon evidence from the Prato Spilla "D" succession, N. Italy. Comptes Rendus De L'academie De Sciences, Paris 315, 1425–1431.
Prentice, I.C., Jolly, D., Participants, B., 2000. Mid-Holocene and Glacial-Maximum vegetation geography of the northern continents and Africa. J Biogeogr 27 (3), 507–519.
QGIS, 2022. QGIS Geographic Information System. Open Source Geospatial Foundation Project. http://qgis.osgeo.org.
Ravazzi, C., 2002. Late Quaternary history of spruce in southern Europe. Rev. Palaeobot. Palynol. 120 (2002), 131–177.
Ravazzi, C., 2005. Il Tardoglaciale: suddivisione stratigrafica, evoluzione sedimentaria e vegetazionale nelle Alpi e in Pianura Padana. Studi Trent. Sci. Nat., Acta Geol. 82, 17–29.
Ravazzi, C., Donegana, M., Vescovi, E., Arpenti, E., Caccianiga, M., Kaltenrieder, P., Londeix, L., Marabini, S., Mariani, S., Pini, R., Vai, G.B., Wick, L., 2006. A new Late-glacial site with *Picea abies* in the northern Apennine foothills: an exception to the model of glacial refugia of trees. Veget. Hist. Archaeobot. 15, 357–371. https://doi.org/10.1007/s00334-006-0055-9.
Regione Emilia-Romagna, 2020. Topographic Database —. http://geoportale.regione.emilia-romagna.it/it/mapshop/.
Regione, Emilia-Romagna, 2021. Landslide Inventory Map and Landslides Historical Archive. https://ambiente.regione.emilia-romagna.it/it/geologia/cartografia/webgis-banchedati/cartografia-dissestoidrogeologico.
Reimer, P.J., Austin, W.E.N., Bard, E., Bayliss, A., Blackwell, P.G., Bronk Ramsey, C., Butzin, M., Cheng, H., Edwards, R.L., Friedrich, M., Grootes, P.M., Guilderson, T.P., Hajdas, I., Heaton, T.J., Hogg, A.G., Hughen, K.A., Kromer, B., Manning, S.W., Muscheler, R., Palmer, J.G., Pearson, C., van der Plicht, J., Reimer, R.W., Richards, D.A., Scott, E.M., Southon, J.R., Turney, C.S.M., Wacker, L., Adolphi, F., Büntgen, U., Capano, M., Fahrni, S.M., Fogtmann-Schulz, A., Friedrich, R., Köhler, P., Kudsk, S., Miyake, F., Olsen, J., Reinig, F., Sakamoto, M., Sookdeo, A.,

Talamo, S., 2020. The IntCal20 Northern Hemisphere radiocarbon age calibration curve (0–55 cal kBP). Radiocarbon 62 (4), 725–757. https://doi.org/10.1017/RDC.2020.41.

Rita, A., Saracino, A., Cieraad, E., Saulino, L., Zotti, M., Idbella, M., De Stefano, C., Mogavero, V., Allevato, E., Bonanomi, G., 2023. Topoclimate effect on treeline elevation depends on the regional framework: A contrast between Southern Alps (New Zealand) and Apennines (Italy) forests. Ecol. Evol. 13 https://doi.org/10.1002/ece3.9733.

Roering, J., 2012. Tectonic geomorphology: landslides limit mountain relief. Nat. Geosci. 5, 446–447.

Segadelli, S., Grazzini, F., Rossi, V., Aguzzi, M., Marvelli, S., Marchesini, M., Chelli, A., Francese, R., De Nardo, M.T., Nanni, S., 2020. Changes in high-intensity precipitation on the northern Apennines (Italy) as revealed by multidisciplinary data over the last 9000 years. Clim. past 16, 1547–1564. https://doi.org/10.5194/cp-16-1547-2020.

Soldati, M., Corsini, A., Pasuto, A., 2004. Landslides and climate change in the Italian Dolomites since the Late glacial. Catena 55, 141–161. https://doi.org/10.1016/S0341-8162(03)00113-9.

Soldati, M., Borgatti, L., Cavallin, A., De Amicis, M., Frigerio, S., Giardino, M., Mortara, G., Pellegrini, G.B., Ravazzi, C., Surian, N., Tellini, C., Zanchi, A., 2006. Geomorphological evolution of slopes and climate changes in Northern Italy during the late Quaternary: spatial and temporal distribution of landslides and landscape sensitivity implications. Geografia Fisica Dinamica Quaternaria 29, 153–163.

Stuiver, M., Reimer, P.J., Reimer, R.W., 2022. CALIB 8.2, software program at http://calib.org, accessed 2022-04-30.

Tellini, C., Chelli, A., 2003. Ancient and recent landslide occurrences in the Emilia Apennines (Northern Apennines, Italy). In: Castaldini, D., Gentili, B., Materazzi, M., Pambianchi, G. (Eds.), Proceedings of the workshop 'Geomorphological sensitivity and system response'. Camerino 4-9 July 2003, 105-114.

Vescovi, E., Ammann, B., Ravazzi, C., Tinner, W., 2010. A new Late-glacial and Holocene record of vegetation and fire history from Lago del Greppo, northern Apennines, Italy. Vegetation History and Archaeobotany 19, 219–233.

Walker, M., Gibbard, P., Head, M.J., Berkelhammer, M., Björck, S., Cheng, H., Cwynar, L. C., Fisher, D., Gkinis, V., Long, A., Lowe, J., Newnham, R., Rasmussen, S.O., Weiss, H., 2019. Formal Subdivision of the Holocene Series/Epoch: A Summary. J. Geol. Soc. India 93, 135–141. https://doi.org/10.1007/s12594-019-1141-9.

Watson, C.S., 1996. The vegetational history of the northern Apennines, Italy: information from three new sequences and a review of Regional vegetational change. J. Biogeogr. I1996 (23), 805–841. https://doi.org/10.1111/j.1365-2699.1996.tb00041.x.